Phase synchronization:
from theory to data analysis

Michael Rosenblum [a], Arkady Pikovsky [a], Jürgen Kurths [a]
Carsten Schäfer [b], and Peter A. Tass [c]

[a] *Department of Physics, University of Potsdam,*
Am Neuen Palais 10, D-14415 Potsdam, Germany
URL: www.agnld.uni-potsdam.de

[b] *Centre for Nonlinear Dynamics, Department of Physiology,*
McGill University, 3655 Drummond Street, Montreal, Quebec H3G lY6, Canada
[c] *Institute of Medicine (MEG), Research Centre Jülich, D-52425 Jülich, Germany*

Abstract

Synchronization of coupled oscillating systems means appearance of certain relations between their phases and frequencies. Here we use this concept in order to address the inverse problem and to reveal interaction between systems from experimental data. We discuss how the phases and frequencies can be estimated from time series and present techniques for detection and quantification of synchronization. We apply our approach to human posture control data of healthy subjects and neurological patients, to multichannel magnetoencephalography data and records of muscle activity of a Parkinsonian patient, and also use it to analyse the cardiorespiratory interaction in humans. By means of these examples we demonstrate that our method is effective for the analysis of systems interrelation from noisy nonstationary bivariate data and provides other information than traditional correlation (spectral) techniques.

Contents

1 Introduction

Synchronization is a basic phenomenon in science, discovered at the beginning of the modern scientific age by Huygens [1]. In the classical sense, synchronization means adjustment of frequencies of periodic self-sustained oscillators due to weak interaction [2–5]. This effect (also referred to as *phase locking* or *frequency entrainment*) is well studied and finds a lot of practical applications [3,4].

During the last 15 years the notion of synchronization has been generalized to the case of interacting chaotic oscillators. In this context, different phenomena exist which are usually referred to as "synchronization", so one needs a more precise description. Due to a strong interaction of two (or a large number) of identical chaotic systems, their states can coincide, while the dynamics in time remains chaotic [6,7]. This effect can be denoted as "complete (identical) synchronization" of chaotic oscillators. It can be easily generalized to the case of slightly non-identical systems [7], or the interacting subsystems [8].

Recently, the effect of *phase synchronization* of chaotic systems has been described [9]. It is mostly close to synchronization of periodic oscillations, where only the phase locking is important, while no restriction on the amplitudes is imposed. Correspondingly, the phase synchronization of chaotic system is defined as the appearance of a certain relation between the phases of interacting systems (or between the phase of a system and that of an external force), while the amplitudes can remain chaotic and are, in general, non-correlated. Of course, the very notion of phase and amplitude of chaotic systems is rather non-trivial. Remarkably, the properties of phase synchronization in chaotic systems are similar to those of synchronization in periodic *noisy* oscillators [10]. This allows one to describe both effects within a common framework. Moreover, from the experimentalist's point of view, one can use the same methods in order to detect synchronization in both chaotic and noisy systems; we will use this analogy below. Describing particular experiments and searching for phase synchronization, we will not be interested in the question, whether the observed oscillations are chaotic or noisy: the approach we present below is equally applicable in both these cases.

1.1 Synchronization in biology

Synchronization phenomena are often encountered in living nature. Indeed, the concept of synchronization is widely used in experimental studies and in the modeling of interaction between different physiological (sub)systems demonstrating oscillating behavior. The examples range from the modeling

of the heart in the pioneering paper of van der Pol and van der Mark [11] to investigation of the circadian rhythm [12,13], phase locking of respiration with a mechanical ventilator [14] or with locomotory rhythms [15], coordinated movement [13] and animal gaits [16], phase locking of chicken embrion heart cells with external stimuli and interaction of sinus node with ectopic pacemakers [13], synchronization of oscillations of human insulin secretion and glucose infusion [17], locking of spiking from electroreceptors of a paddlefish to weak external electromagnetic field [18], and synchronization of heart rate by external audio or visual stimuli [19].

A very interesting and important example is interaction of human cardiovascular and respiratory systems. Although it is well-known that these systems do not act independently [20] and in spite of early communications in the medical literature (that often used different terminology) [21–26], in the biological physics community these two systems were often considered to be not synchronized. So, an extensive review of previous studies of biological rhythms led to the conclusion that "there is comparatively weak coupling between respiration and the cardiac rhythm, and the resulting rhythms are generally not phase locked" (see [13], page 136). Recently, the interaction of these vital systems attracted attention of several physics groups, and synchronization during paced respiration [27,28] was investigated. Here, as well as in Refs. [21,23,24,27,28] only synchronous states of orders $n : 1$ (n heartbeats within 1 respiratory cycle) were found due to limitation of the *ad hoc* methods used for the analysis of data. In our recent work [29,30] we have reported on cardiorespiratory synchronization under free-running conditions; the proposed analysis technique allows to find out synchronous epochs of different orders $n : m$. This finding gives some indication for the existence of an unknown form of cardiorespiratory interaction.

The notion of synchronization is also related to several central issues of neuroscience (see, e.g., [31]). For instance, synchronization seems to be a central mechanism for neuronal information processing within a brain area as well as for communication between different brain areas. Results of animal experiments indicate that synchronization of neuronal activity in the visual cortex appears to be responsible for the binding of different but related visual features so that a visual pattern can be recognized as a whole [32–34,31]. Another evidence is that synchronization of the oscillatory activity in the sensorimotor cortex may serve for the integration and coordination of information underlying motor control [35]. Moreover, synchronization between areas of the visual and parietal cortex, and between areas of the parietal and motor cortex was observed during a visuomotor integration task in an awake cat [36]. However, as yet, little is known about synchronization between different brain areas and its functional role and behavioral correlates in humans. On the other hand, synchronization plays an important role in several neurological diseases like epilepsies [37] and pathological tremors [38,39]. Correspondingly, it is impor-

tant to analyze such synchronization processes to achieve a better understanding of physiological brain functioning as well as disease mechanisms.

1.2 Synchronization and analysis of bivariate data

As we have argued above, synchronization phenomena are abundant in the real world and biological systems, in particular. Thus, detection of synchronization from experimental data appears to be an important problem, that can be formulated as follows: Suppose we can obtain several signals coming from different simultaneous measurements (e.g., an electrocardiogram and respiratory movements, multichannel electro- or magnetoencephalography data, records of muscle activity, etc.). Usually it is known how to attribute these signals to different oscillating objects. The question is whether there are states (or epochs) where these objects oscillate in synchrony. Unfortunately, typically observed oscillations are highly irregular, especially in live systems, and therefore possible synchronization phenomena are masked by strong noise and/or chaos, as well as by nonstationarity.

This task is similar to a well-known problem in time series analysis: how to reveal the presence of an interdependence between two (or more) signals. The analysis of such bivariate data is traditionally done by means of linear cross-correlation (cross-spectrum) techniques [40] or nonlinear statistical measures like mutual information or maximal correlation [41–43].

Recently, different synchronization concepts of nonlinear dynamics have been used in studies of bivariate data. Schiff et al. [44] used the notion of dynamical interdependence [45] and applied the mutual prediction technique to verify the assumption that measured bivariate data originate from two synchronized systems, where synchronization was understood as the existence of a functional relationship between the states of two systems, called generalized synchronization. In our previous works [46–49,29], we proposed an ansatz based on the notion of phase synchronization; this implies existence of a relationship between phases of two weakly interacting systems, whereas the amplitudes may remain uncorrelated [9,10]. In our approach we assume that the measured bivariate data originate from two interacting self-oscillatory systems which may either be phase locked or oscillate independently.

Generally, we try to access the following problem: suppose we observe a system with a complex structure that is not known exactly, and measure two time series at its outputs (Fig. 1). Our goal is not only to find out whether these signals are dependent or not - this can be done by means of traditional statistical techniques - but to extract additional information on the interaction of some subsystems within the systems. Obviously, we cannot consider

the system under study as a "black box", but need some additional knowledge to support the assumption that the content of this "box" is complex, and we indeed encounter several subsystems, that generate their own rhythms, but are, probably, weakly coupled.

An advantage of our approach is that it allows to address rather weak interaction between the two oscillatory subsystems. Indeed, the notion of phase synchronization implies only some interdependence between phases, whereas the irregular amplitudes may remain uncorrelated. The irregularity of amplitudes can mask the phase locking so that traditional techniques treating not the phases but the signals themselves may be less sensitive in the detection of the systems' interrelation [46,48].
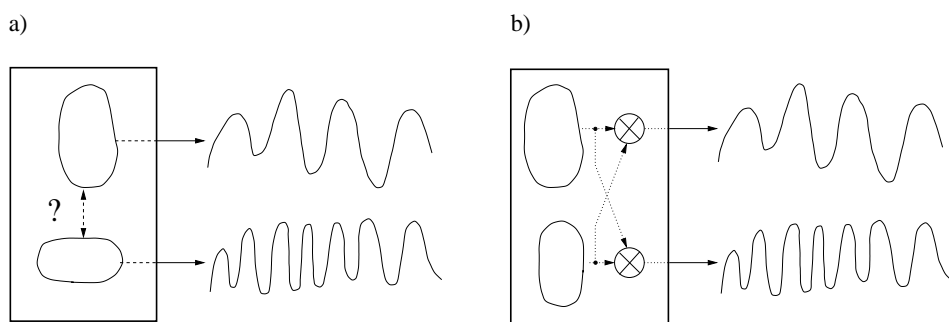

Fig. 1. Illustration of the synchronization approach to analysis of bivariate data. The goal of the analysis is to reveal the presence of a weak interaction between two subsystems from the signals at their outputs only. The assumption made is that the data are generated by two oscillators having their own rhythms (a). An alternative hypothesis is a mixture of signals generated by two uncoupled systems (b).

In the following we briefly review the ideas and results of theoretical studies of the synchronization phenomena that are used in our approach to time series analysis. Next, we present techniques of the bivariate data analysis and illustrate them by examples of physiological data. These examples are given in the ascending order of the signal analysis complexity, and in our presentation we dwell on the analysis itself, but not on the physiological importance of the results.

2 Phase and frequency locking: a brief review

We know that synchronization of weakly coupled oscillators appears as some relation between their phases and frequencies. In the context of data analysis we are going to exploit this fact to tackle the inverse problem: our goal is to reveal the presence of synchronization from the data. To this end we have to estimate from the signals the phases and frequencies and analyse the

relations between them. First, we summarize what we know about the interdependence of phases and frequencies of synchronized systems. Definitely, as the experimental data are inevitably noisy, we always have to take fluctuations into account. Therefore, any relation between phases should be treated in a statistical sense.

2.1 Periodic oscillators

Stable periodic self-sustained oscillations are represented by a stable limit cycle in the phase space, and the dynamics of a phase point on this cycle can be described as

$$\frac{d\phi}{dt} = \omega_0 \ , \tag{1}$$

where $\omega_0 = 2\pi/T_0$, and T_0 is the period of the oscillation. It is important that starting from any monotonically growing variable θ on the limit cycle, one can introduce the phase satisfying Eq. (1). Indeed, an arbitrary θ obeys $\dot{\theta} = \nu(\theta)$ with a periodic $\nu(\theta + 2\pi) = \nu(\theta)$. A change of variables

$$\phi = \omega_0 \int\limits_0^\theta [\nu(\theta)]^{-1} d\theta$$

gives the correct phase, where the frequency ω_0 is defined from the condition $2\pi = \omega_0 \int_0^{2\pi} [\nu(\theta)]^{-1} d\theta$. A similar approach leads to correct angle-action variables in Hamiltonian mechanics. From (1) it is evident that the phase corresponds to the zero Lyapunov exponent, while negative exponents correspond to the amplitude variables (not written in (1)).

If two oscillators are weakly coupled, then in the first approximation one can neglect variations of the amplitudes to obtain equations describing the phase dynamics. In general, these equations have the form

$$\frac{d\phi_1}{dt} = \omega_1 + \varepsilon g_1(\phi_1, \phi_2) \ , \qquad \frac{d\phi_2}{dt} = \omega_2 + \varepsilon g_2(\phi_2, \phi_1) \ , \tag{2}$$

where the coupling terms $g_{1,2}$ are 2π-periodic in both arguments, and ε is the coupling coefficient.

The phase space of Eqs. (2) is a 2-torus, and with the usual construction of the Poincaré map this system can be made equivalent to a circle map, with a well-known structure of phase-locking intervals (Arnold's tongues) [50]; each of the intervals corresponds to a $n : m$ synchronization region. This picture is

7

universal and its qualitative features do not depend on the characteristics of the oscillations and of the external force (e.g. nearly sinusoidal or relaxational), and on the relation between amplitudes.

Analytically, one can proceed as follows. The interaction between the oscillators essentially effects the evolution of their phases if the frequencies $\omega_{1,2}$ are in resonance, i.e. if for some integers n, m we have

$$n\omega_1 \approx m\omega_2 .$$

Then, in the first approximation, the Fourier expansion of the functions $g_{1,2}$ contains slowly varying terms $\sim n\phi_1 - m\phi_2$. This suggests to introduce the *generalized phase difference*,

$$\varphi_{n,m}(t) = n\phi_1(t) - m\phi_2(t) . \tag{3}$$

Subtracting the equations (2) and keeping only the resonance terms, we get

$$\frac{d\varphi_{n,m}}{dt} = n\omega_1 - m\omega_2 + \varepsilon G(\varphi_{n,m}) , \tag{4}$$

where $G(\cdot)$ is 2π-periodic. This is a one-dimensional ODE that admits solutions of two kinds: fixed points or periodic rotations of $\varphi_{n,m}$. The stable fixed point corresponds to perfect phase locking $\varphi_{n,m} = const$; periodic rotations describe quasiperiodic motion with two incommensurate frequencies in the system (2).

In the analytical treatment of the Eqs. (2) we have neglected nonresonant terms, what is justified for small coupling. With nonresonant terms, the condition of synchronization for periodic oscillators should be generally written as a phase locking condition

$$|n\phi_1(t) - m\phi_2(t) - \delta| < \text{const} \tag{5}$$

where δ is some (average) phase shift, or as a frequency entrainment condition

$$n\Omega_1 = m\Omega_2 , \tag{6}$$

where

$$\Omega_{1,2} = \langle \frac{d\phi_{1,2}}{dt} \rangle .$$

We emphasize, that in the synchronized state the phase difference is generally not constant but oscillates around δ. These oscillations vanish in the limit of very small coupling (correspondingly, the frequency mismatch $n\omega_1 - m\omega_2$

8

must be also small), or if the coupling depends only on the relative phase:
$g_{1,2} = g_{1,2}(n\phi_1 - m\phi_2)$.

2.2 Noisy oscillators

In general, both properties of phase and frequency locking (Eqs. (5,6)) are destroyed in the presence of noise $\xi(t)$ when instead of (4) one has

$$\frac{d\varphi_{n,m}}{dt} = n\omega_1 - m\omega_2 + \varepsilon G(\varphi_{n,m}) + \xi(t) \ . \tag{7}$$

For small noise the stable phase dynamics is only slightly perturbed. Thus the relative phase $\varphi_{n,m}$ mainly fluctuates around some constant level (former fixed point). These nearly stationary fluctuations may be interrupted by phase slips, where the relative phase changes relatively rapidly by $\pm 2\pi$. Thus, strictly speaking, the phase difference is unbounded and condition (5) is not valid anymore. Nevertheless, the distribution of the *cyclic relative phase*

$$\Psi_{n,m} = \varphi_{n,m} \bmod 2\pi \tag{8}$$

has a dominating peak around the value corresponding to the stable fixed point [51]. Presence of this peak can be understood as the phase locking in a statistical sense.

If the noise is weak and *bounded*, then the phase slips are impossible and there exists a range of frequency mismatch $n\omega_1 - m\omega_2$, where the averaged condition of frequency locking (6) is fulfilled. Near the boundaries of the Arnold tongue the noise causes phase slips and the transition out of the synchronous regime is now smeared. If the noise is unbounded, e.g. Gaussian, the probability of a slip to occur is nonzero even for $n\omega_1 - m\omega_2 = 0$, so that strictly speaking the region of frequency locking shrinks to a point. As this probability is (exponentially) small for weak noise, practically the synchronization region appears as an interval of $n\omega_1 - m\omega_2$ where $n\Omega_1 \approx m\Omega_2$. Within this region, the distribution of the cyclic relative phase is not uniform, so that one can speak of phase locking.

In the case of strong noise, the phase slips in both directions occur very frequently, so that the segments of nearly constant relative phase are very short and time course of $\varphi_{n,m}(t)$ looks like a random walk, that is unbiased in the very center of the synchronization region and biased otherwise. The synchronization transition is now completely smeared and, hence, synchronization appears only as a weakly seen tendency.

For the periodic oscillator the phase was introduced in Eq. (1) as a variable corresponding to the shift along the limit cycle, and, hence, to the zero Lyapunov exponent. Any autonomous continuous-time dynamical system with chaotic behaviour possesses one zero Lyapunov exponent that correspond to shifts along the flow, therefore we expect that phase can be defined for this case as well.

Suppose we can define a Poincaré secant surface for our autonomous continuous-time system. Then, for each piece of a trajectory between two cross-sections with this surface we define the phase as a piece-wise linear function of time, so that the phase increment is 2π at each rotation:

$$\phi_P(t) = 2\pi \frac{t - t_n}{t_{n+1} - t_n} + 2\pi n, \qquad t_n \leq t < t_{n+1}. \tag{9}$$

Here t_n is the time of the n-th crossing of the secant surface. Obviously, the definition is ambiguous, because it crucially depends on the choice of the Poincaré surface. Nevertheless, defined in this way, the phase has a physically important property: its perturbations neither grow nor decay in time, so it does correspond to the direction with the zero Lyapunov exponent in the phase space. Note that for periodic oscillations corresponding to a fixed point of the Poincaré map, this definition gives the correct phase satisfying Eq. (1).

In contrast to the case of periodic oscillations, the growth of the phase of a chaotic system cannot generally be expected to be uniform. Instead, the instantaneous frequency depends in general on the coordinate of the intersection with the Poincaré surface, i.e. on the irregular amplitude. This dependence can be considered as an influence of some effective "noise" (although this irregularity has of course purely deterministic origin). Thus, the synchronization phenomena for chaotic system are similar to those in noisy periodic oscillations [9,10], therefore, from an experimentalist's viewpoint, we can treat them in the same way.

2.4 An example: two coupled noisy Rössler oscillators

For illustration we take two coupled chaotic Rössler oscillators subject to noisy perturbations. Namely, we consider the model

$$\dot{x}_{1,2} = -\omega_{1,2}y_{1,2} - z_{1,2} + \xi_{1,2} + \varepsilon(x_{2,1} - x_{1,2})$$
$$\dot{y}_{1,2} = \omega_{1,2}x_{1,2} + 0.15y_{1,2} \qquad\qquad (10)$$
$$\dot{z}_{1,2} = 0.2 + z_{1,2}(x_{1,2} - 10)$$

where the parameters $\omega_{1,2} = 1 \pm \Delta\omega$ and ε govern the frequency mismatch and the strength of coupling, respectively; $\xi_{1,2}$ are two Gaussian delta-correlated noise terms fulfilling $\langle \xi_i(t)\xi_j(t') \rangle = 2D\delta(t - t')\delta_{i,j}$. The system is simulated by Euler's technique with the time step $\Delta t = 2\pi/1000$. In the following we fix $D = 1$.
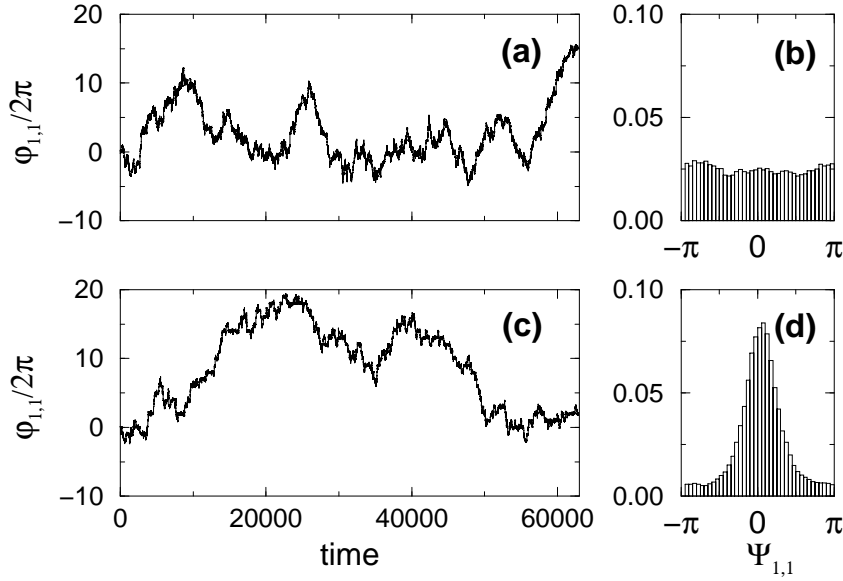

Fig. 2. Relative phase $\varphi_{1,1} = \phi_1 - \phi_2$ and distribution of $\Psi_{1,1} = \varphi_{1,1} \bmod 2\pi$ for the case of uncoupled (a,b) and coupled (c,d) identical chaotic systems perturbed by noise. Although the fluctuations of $\varphi_{1,1}$ in both cases seem to be quite alike, the distributions (b) and (d) clearly identify the difference between coupled and uncoupled regimes.

First we consider the case of two identical oscillators, i.e. $\Delta\omega = 0$. It makes no sense to speak of frequency locking here, as the averaged frequencies are equal even if the oscillators are uncoupled. Nevertheless, we can distinguish the uncoupled ($\varepsilon = 0$) and coupled cases ($\varepsilon = 0.04$) if we look at the distribution of the relative phase (Fig. 2). In both cases the relative phase performs a random-walk-like motion, but its distribution is uniform in the absence of

11

coupling and has a well-expressed peak if two systems weakly interact. Thus, in the latter case we encounter phase locking understood in a statistical sense.

Now we consider detuned oscillators, $\Delta\omega = 0.015$ (Fig. 3). In the absence of noisy perturbations, the phase difference oscillates around some constant level, and its distribution obviously has a sharp peak (not shown). Therefore we can speak of frequency and phase locking here (Fig. 3c). In the presence of noise the relative phase performs a biased random walk, so there is obviously no frequency locking. Nevertheless, the distribution of the phase definitely shows the presence of phase locking (Fig. 3).
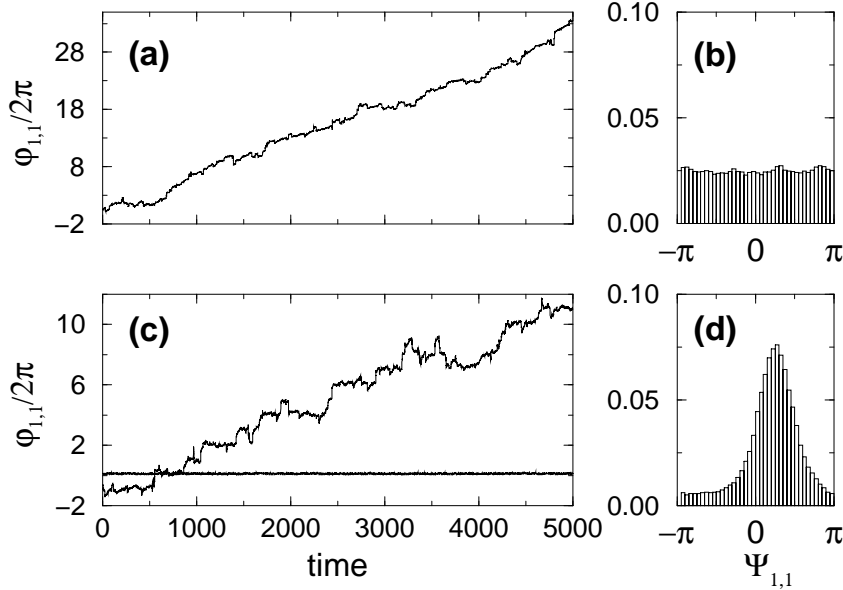

Fig. 3. Relative phase $\varphi_{1,1} = \phi_1 - \phi_2$ and distribution of $\Psi_{1,1} = \varphi_{1,1} \bmod 2\pi$ for the case of uncoupled (a,b) and coupled (c,d) non-identical chaotic systems perturbed by noise. The horizontal line in (c) corresponds to the absence of noise: in this case the phase difference fluctuates around some constant value due to influence of chaotic amplitudes. These fluctuations are rather small (barely seen in this scale), and no phase slips are observed; this fact is explained by the high phase coherence properties of the Rössler attractor. In contrast to the noisy case, here we observe both frequency and phase locking.

To conclude this Section, we stress that the appearance of synchronization entails some relations between phases and frequencies of oscillators, but the inverse statement is strictly speaking not correct. Indeed, if a system is outside the synchronization region, but close to its border, then the distribution of the cyclic relative phase is also non-uniform, and the frequencies of oscillators are closer than those for non-interacting systems. Thus, the presence of a peak in the distribution of $\Psi_{n,m}(t)$ generally indicates the presence of some interaction only, but does not necessarily mean that the systems are synchronized. As we are not interested in determination of the borders of a synchronization region,

but are only searching for the presence of coupling, this fact does not influence interpretation of our results.

3   Estimating phases from data

Before we can analyse the relations between the phases of two oscillators, we have to estimate these phases from scalar signals. We have shown above how to define the phase for a periodic self-sustained system and for chaotic oscillations. Quite often, the phase of an oscillator can be determined if one can find a suitable projection of the phase space ensuring that all the trajectories rotate around some point that is taken as the origin. From this projection, the phase can be identified with the angle (with respect to an arbitrary direction) of the vector drawn from the origin to the corresponding point on the trajectory. Note that in this way we obtain a some non-uniformly rotating phase, what can essentially complicate the analysis. Another possibility is to construct a Poincaré map (stroboscopic map) and to define the phase according to (9).
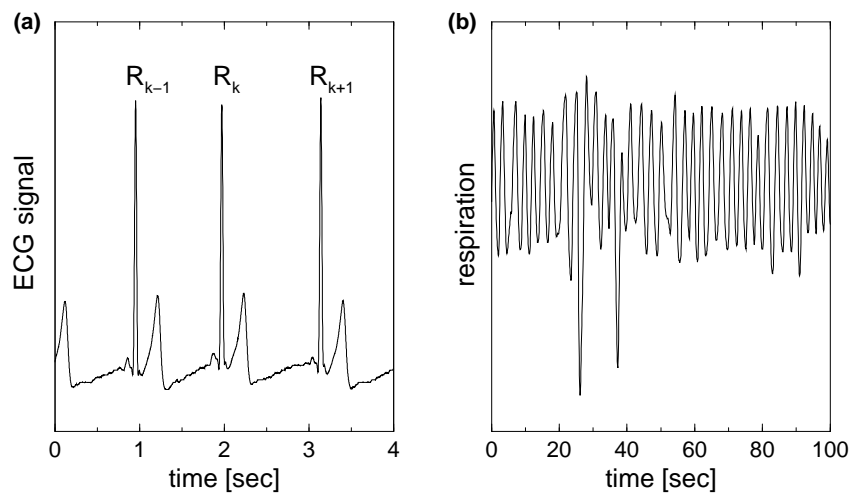

Fig. 4. Short segments of an electrocardiogram with the R-peaks marked (a) and of a respiratory signal (b); both signals are in arbitrary units.

These two methods can be adapted for estimation of phases from experimental data. To explain the details, we consider a human electrocardiogram (ECG) and a respiratory signal (air flow measured at the nose of the subject) as examples. An essential feature of the ECG is that every (normal) cardiocycle contains a well-pronounced sharp peak that can be with high precision localized in time; traditionally it is denoted as R-peak (Fig. 4a). The series of R-peaks can be considered as a sequence of point events taking place at times t_k, $k = 1, 2, \ldots$. Phase of such a process can be easily obtained. Indeed, the time interval between two R-peaks corresponds to one complete cardiocycle [1];

---

[1] From the physiologist's viewpoint the cardiocycle starts with the P-wave that

13

therefore the phase increase during this time interval is exactly 2π. Hence, we can assign to the times t_k the values of phase $\phi(t_k) = 2\pi k$, and for arbitrary instant of time $t_k < t < t_{k+1}$

$$\phi(t) = 2\pi k + 2\pi \frac{t - t_k}{t_{k+1} - t_k} \; .$$ (11)

This method can be applied to any process that contains distinct marker events and can therefore be reduced to the spike train. Determination of the phase via marker events in time series can be considered as the analogy to the technique of Poincaré section, although we do not need to assume that the system under study is a dynamical one.

Now we consider the respiratory signal (Fig. 4b); it reminds a sine-wave with slowly varying frequency and amplitude. Phase of such a signal can be obtained by means of the *analytic signal concept* originally introduced by Gabor in 1946 [52]. To implement it, one has to construct from the scalar signal $s(t)$ a complex process

$$\zeta(t) = s(t) + \imath s_H(t) = A(t)e^{\imath\phi(t)} \; ,$$ (12)

where $s_H(t)$ is the Hilbert transform (HT) of $s(t)$; the *instantaneous* phase $\phi(t)$ and amplitude $A(t)$ of the signal are then uniquely determined from (12). Note, that although formally this can be done for an arbitrary $s(t)$, $A(t)$ and $\phi(t)$ have clear physical meaning only if $s(t)$ is a narrow-band signal (see the discussion of properties and practical implementation of the HT and analytic signal in the Appendix).

We can look at this technique from the other viewpoint: it can be considered as a two-dimensional embedding in coordinates $(s(t), s_H(t))$. Note, that in these coordinates a harmonic oscillation is represented by a circle for any ω. This circle can be considered as the analogy to the phase portrait of the harmonic oscillator. The phase obtained from this portrait increase linearly in time $\phi(t) = \omega t + \phi_0$, as we expect it for this system. Note, however, that the often used coordinates $(s(t), \dot{s}(t))$ and delay coordinates $(s(t), s(t - \tau))$ generally produce an ellipse; the phase obtained as an angle from such plots demonstrates periodic deviation from the linear growth (i.e., $[\phi(t) - \omega t]$ oscillates periodically) that is in this case the artifact of calculation [2].

_____

reflects the beginning of the excitation in the atria. This does not contradict to our procedure: we understand the cycle as the interval between two nearly identical states of the system.

[2] Obviously, to obtain for a harmonic signal a circle in the embedding one can use the coordinates $(s(t), \dot{s}(t)/\omega)$ or delay coordinates with $\tau = \pi/(2\omega)$, but this requires a priory knowledge of ω and cannot be implemented for a signal with slowly

14

An important practical question is: Which method should be chosen for analysis of particular experimental data? To address this problem we make the following remarks:

- If we define the phase of a system in order to characterize its frequency locking properties, then different methods (via the Poincaré section, from the two-dimensional projection of the phase space or from an oscillatory observable by means of the Hilbert transform) give similar results, at least if the system is a "good" one [10]. Although these phases vary microscopically, i.e. on the time scale less than one (quasi)period, the average frequencies obtained from these phases coincide, and it is exactly the frequencies what is primarily important for the description of synchronization. Therefore, theoretically all the definitions of the phase are equivalent. That is rarely the case in an experimental situation, where we have to estimate the phases from short, noisy and nonstationary records, so that numerical problems become a decisive factor.
- If the signal has very well-defined marker events, like the ECG, the Poincaré-map-technique is the best choice. It could be also applied to an "oscillatory" signal, like the respiratory one: here it is also possible to define the "events" (e.g. as the times of zero crossing) and to compute the phase according to Eq. (11). However, we do not recommend to do this: the drawback is that the determination of an event from the slowly varying signal is strongly influenced by noise and trends in the signal. Besides, we get only one event per quasiperiod, and if the record is short, then the statistics is poor. In such case the technique based on the Hilbert transform is much more effective because it provides the phase for every point of the time series, so that we have a lot of points per quasiperiod and can therefore smooth out the influence of noise and obtain sufficient statistics for the determination of phase relationships.

Another important point is that even if we can unambiguously compute the phase of a signal, we cannot avoid the uncertainty in the determination of the phase of an oscillator [3]. The latter depends on the observable used; "good" observables provide equivalent phases (i.e. the average frequencies defined from these observables coincide). In an experiment we are rarely free in the choice of an observable. Therefore, one should always be very careful in formal application of the presented methods and in the interpretation of the results.

We emphasize, that even if the observable is good enough, the distribution of the estimated cyclic relative phase can essentially differ from that obtained from the correct phase satisfying Eq. (1). Indeed, let us consider a strongly

————

varying frequency.

[3] We remind that although one can compute several phases from different observables of the same oscillator, there exist only one phase of that system corresponding to its zero Lyapunov exponent.

nonlinear limit cycle oscillator and estimate the phase by means of the Hilbert transform, or take as the phase the angle in the phase plane. If the angle velocity of the phase point is essentially non-uniform in time, then the estimated relative phase strongly oscillates on the time scale less than the period of oscillations. In this case the distribution of the cyclic relative phase becomes not unimodal; the presence of noise makes this distribution even more smeared. From the other hand, if the oscillations are nearly harmonic (in this case we call the oscillators quasilinear), then the estimated phase is close to the true one, and the distribution of the cyclic relative phase has a sharp peak. Deviation of the distribution from a unimodal one can also occur if the interaction between oscillators is not weak. We illustrate this with the following example.

An example: Synchronization via parametric action (modulation)

We consider a noisy van der Pol oscillator with modulated natural frequency

$$\ddot{x} - \mu(1 - x^2)\dot{x} + (\omega + \Delta \sin \nu t)^2 x = \xi , \qquad (13)$$

where $\mu = 1$, the natural frequency is $\omega = 1$, and ξ is the Gaussian delta-correlated noise term. We vary the modulating frequency ν around $1/3$, and look for the $1 : 3$ locking.
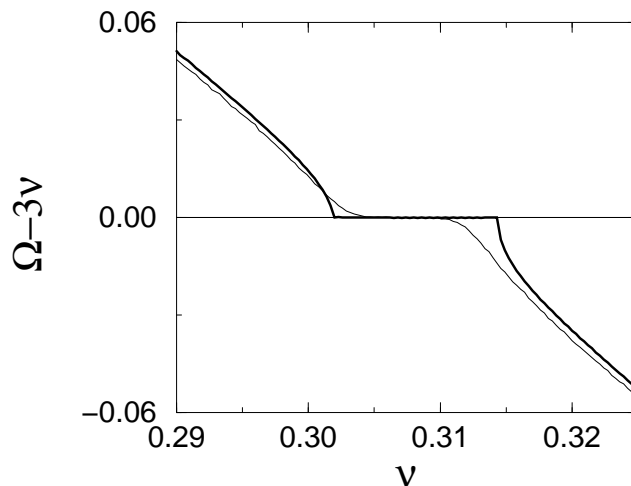

Fig. 5. Frequency — detuning plot for the van der Pol oscillator with the modulated natural frequency; $\Delta = 0.6$. Bold line corresponds to the noise-free case; rather small noise ($D = 0.05$) smears the plateau in the ($\Omega - 3\nu$) vs. ν plot (solid line).

First we compute the averaged frequency of the van der Pol oscillator $\Omega = \langle \dot{\phi}_{vdP} \rangle$ for different values of the modulating frequency ν and plot $\Omega - 3\nu$ vs ν; these dependencies for the noise-free and noisy cases are demonstrated in Fig. 5. We note, that in contrast to the case of synchronization by additive

16

forcing, the locking here occurs only if the amplitude of the modulation Δ exceeds some threshold value (or at least the width of the synchronization region below this threshold is vanishingly small).

Next, we compute the distribution of the relative phase at the center of frequency locking region $\nu = 0.307$. These distributions shown in Fig. 6 are not unimodal. Hence, synchronization via parametric modulation cannot be easily described in terms of phase locking understood as the existence of a statistically preferred value of the relative phase. In this case, in order to reveal synchronization from phases, one has to use the stroboscopic approach, i.e. to observe the phase of the oscillator at the instants of time when the phase of the drive attains a certain fixed value; we explain this technique below.
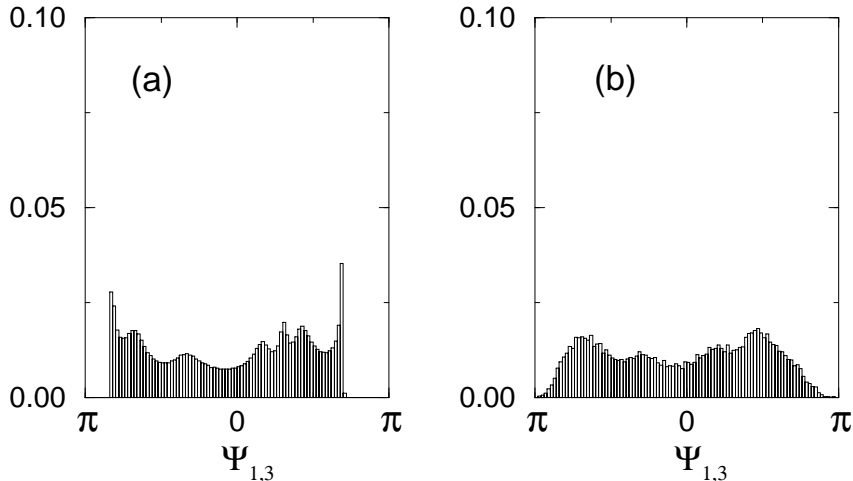

Fig. 6. Distribution of the cyclic relative phase for the noise-free (a) and noisy (b) van der Pol oscillator with the modulated natural frequency.

4 Straightforward analysis of phase difference: Application to posture control

Sometimes synchronization can be detected in a straightforward way: by plotting the generalized phase difference $\varphi_{n,m}$ (see Eq. (3)) versus time and looking for horizontal plateaus in this presentation. This simple method proved to be efficient in investigation of model systems as well as for some experimental data [48,18,19].

To illustrate this, we present the results of experiments on posture control in humans [48]. During these tests a subject is asked to stay quietly on a special rigid force plate equiped with four tensoelectric transducers. The output of the setup provides current coordinates (x, y) of the center of pressure under the feet of the standing subject. These bivariate data are called stabilograms;

they are known to contain rich information on the state of the central nervous system [53–56]. Every subject was asked to perform three tests of quiet upright standing (3 minutes) with
(a) eyes opened and stationary visual surrounding (EO);
(b) eyes closed (EC);
(c) eyes opened and additional video–feedback (AF).
132 bivariate records obtained from 3 groups of subjects (17 healthy persons, 11 subjects with an organic pathology and 17 subjects with a phsychogenic pathology) were analysed by means of cross-spectra and generalized mutual information. It is important that interrelation between body sway in anterior–posterior and lateral directions was found in pathological cases only. Another observation is that stabilograms can be qualitatively rated into two groups: noisy and oscillatory patterns. The latter appear considerably less frequently – only some few per cent of the records can be identified as oscillatory – and only in the case of pathology.

The appearance of oscillatory regimes in stabilograms suggests excitation of self-sustained oscillations in the control system responsible for the maintenance of the constant upright posture; this system is known to contain several nonlinear feedback loops with time delay. From the other hand, the independence of body sway in two perpendicular directions for all healthy subjects and many cases of pathology suggests that two separate subsystems are involved in the regulation of the upright stance. A plausible hypothesis is that when self-sustained oscillations are excited in both these subsystems, synchronization may take place. To test whether the interdependence of two components of a stabilogram may be due to synchronization, we have performed the analysis of the relative phase.

Here we present the results for one trial (female subject, 39 years old, functional ataxia). We can see that in the EO and EC tests the stabilograms are clearly oscillatory (Fig. 7)[4]. The difference between these two records is that with eyes opened the oscillations in two directions are not synchronous during approximately the first 110s, but are phase locked during the last 50s. In the EC test, the phases of oscillations are perfectly entrained during all the time. The behavior is essentially different in the AF test; here no phase locking is observed.

An important advantage of the phase analysis is that by means of $\varphi_{n,m}(t)$ plots one can trace transitions between synchronous and non-synchronous states that are due to nonstationarities in interacting systems and/or coupling

---

[4] In order to eliminate low–frequency trends, a moving average computed over the n–point window was subtracted from the original data. The window length n has been chosen by trial to be equal or slightly larger than the characteristic oscillation period. Its variation up to factor 2 does not effect the results.
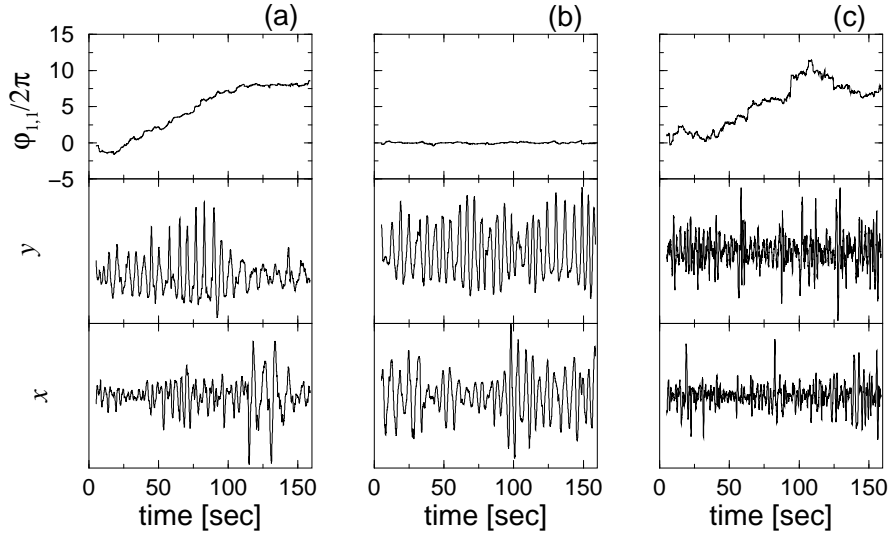
Fig. 7. Stabilograms of a neurological patient for EO (a), EC (b), and AF (c) tests. The upper panels show the relative phase between two signals x and y that are deviation of the center of pressure in anterior–posterior and lateral direction, respectively. During the last 50s of the first test and the whole second test the phases are perfectly locked. No phase entrainment is observed in the AF test.

(Fig. 7a). Noteworthy, this is possible even for very short records. Indeed, two different regimes that can be distinguished in (Fig. 7a) contain only about ten quasiperiods, i.e. these epochs are too short for reliable application of conventional methods of time series analysis.

A disadvantage of the method is that synchronous regimes which correspond to neighboring Arnold tongues, e.g. synchronization of order $n : (m + 1)$, appear in this presentation as nonsynchronous epochs. Besides, there exist no regular methods to pick up the integers n and m, so that they are usually found by trial and error. Respectively, in order to reveal all the regimes, one has to analyse a number of plots. In practice, the possible values of n and m can be estimated from the power spectra of the signals and are often restricted due to some additional knowledge on the system under study.

Another drawback of this technique is that if noise is relatively strong, this method becomes ineffective and may be even misleading. Indeed, frequent phase slips mask the presence of plateaus (cf. Fig. 3) and synchronization can be revealed only by a statistical approach, i.e. by analysis of the distribution of the cyclic relative phase $\Psi_{n,m}$.

19

5 Statistical analysis of phase difference: Application to brain activity

If the interacting oscillators are quasilinear then we can estimate the strength of the $n : m$ phase locking by comparing the distribution of the cyclic relative phase $\Psi_{n,m}(t)$ with the uniform distribution. For a single record this can be done by visual inspection (cf. the example of coupled noisy Rössler oscillators, Figs. 2,3). In order to perform automatized analysis for large data sets or in order to trace the variation of the strength of interaction with variation of some parameter, we need quantitative criteria of synchronization. Quantitative characterization is also required for significance tests. To this end we introduce three $n : m$ *synchronization indices*:

(1) The synchronization index based on the Shannon entropy S of the phase difference distribution [49]. Having an estimate p_k of the distribution of $\Psi_{n,m}$, we define the index ρ as

$$\rho_{n,m} = \frac{S_{max} - S}{S_{max}} \, , \tag{14}$$

where $S = -\sum_{k=1}^{N} p_k \ln p_k$, and the maximal entropy is given by $S_{max} = \ln N$; N is the number of bins and p_k is the relative frequency of finding $\Psi_{n,m}$ within the k-th bin [5]. Due to the normalization used,

$$0 \leq \rho_{n,m} \leq 1 \, , \tag{15}$$

whereas $\rho_{n,m} = 0$ corresponds to a uniform distribution (no synchronization) and $\rho_{n,m} = 1$ corresponds to a distribution localized in one point (δ-function). Such distribution can be observed only in the ideal case of phase locking of noise-free quasilinear oscillators.

(2) Intensity of the first Fourier mode of the distribution

$$\gamma_{n,m}^2 = \langle \cos \Psi_{n,m}(t) \rangle^2 + \langle \sin \Psi_{n,m}(t) \rangle^2 \, , \tag{16}$$

where the brackets denote the average over time, can serve as the other measure of the synchronization strength; it also varies from 0 to 1. The advantage of this index is that its computation involves no parameters: we do not need to choose the number of bins as we do not calculate the distribution itself.

(3) If the oscillators are strongly nonlinear then the distribution of $\Psi_{n,m}(t)$ is non-uniform even in the absence of noise; this is essential if synchronization occurs via parametric action. In this case we need some other measure to characterize the strength of synchronization. For this purpose we

---

[5] The optimal number of bins can be estimated as $N = \exp[0.626 + 0.4 \ln(M - 1)]$, where M is the number of samples [57].

recall the stroboscopic approach: we know that in the synchronous state the distribution of the stroboscopically observed phase is the δ-function; it is smeared in the presence of noise. Thus, for $n : m$ synchronization we have to characterize the distribution of

$$\eta = \phi_2 \bmod 2\pi n \left|_{\phi_1 \bmod 2\pi m = \theta}\right. \; . \tag{17}$$

This means that we observe the phase of the second oscillator at the instants of time when the phase of the first one attains a fixed value θ (phase stroboscope). To account for the $n : m$ locking, the phases are wrapped into intervals $[0, 2\pi m]$ and $[0, 2\pi n]$, respectively. Repeating this procedure for all $0 \leq \theta < 2\pi$ and averaging, we get a statistically significant synchronization index [49].
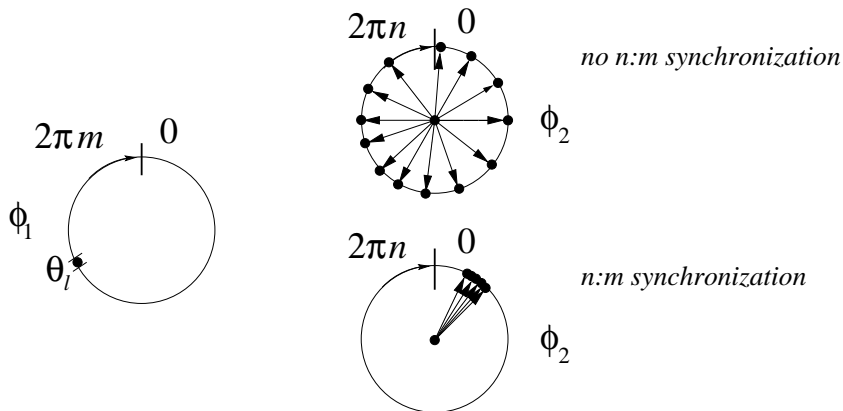

Fig. 8. Synchronization index based on the conditional probability. Phase of the second oscillator ϕ_2 wrapped in the interval $[0, 2\pi n]$ is observed stroboscopically, i.e. when phase of the first oscillator ϕ_1 is found in the certain bin θ_l of the interval $[0, 2\pi m]$. If there is no synchronization then the stroboscopically observed ϕ_2 is scattered over the circle, otherwise it groups around some value. The sum of the vectors pointing to the position of the phase on the circle provides a quantitative measure of synchronization.

Practically, if we deal with the time series, we can introduce binning for the phase of the first oscillator, i.e. divide the interval $[0, 2\pi m]$ into N bins. Next, we denote the values of $\phi_1 \bmod 2\pi m$ falling into the l-th bin as θ_l and the number of points within this bin as M_l. Then, with the help of Eq. (17) we compute M_l corresponding values $\eta_{i,l}$, where $i = 1, \ldots, M_l$. If the oscillators are not synchronized, then we expect $\eta_{i,l}$ to be uniformly distributed on the interval $[0, 2\pi n]$, otherwise these quantities group around some value and their distribution is unimodal (Fig. 8). To quantify it, we compute

$$\Lambda_l = M_l^{-1} \sum_{i=1}^{M_l} \exp\left[\imath(\eta_{i,l}/n)\right] \; . \tag{18}$$

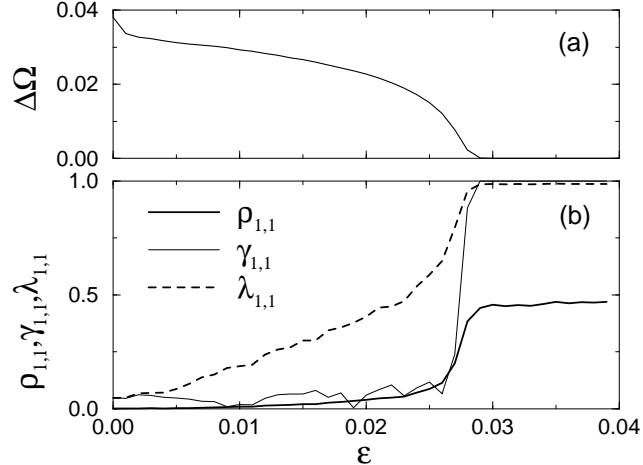The case of complete dependence between both phases corresponds to

21

Fig. 9. Comparison of quantitative measures of synchronization using the simulated data from two coupled Rössler oscillators (Eq. (10)). Transition to synchronous state takes place when the difference of frequencies of two oscillators vanishes with increase of coupling coefficient ε (a). Three $1:1$ synchronization indices are shown as the functions of ε (b).

$|\Lambda_l| = 1$, whereas $|\Lambda_l|$ vanishes if there is no dependence at all. To improve the statistics, we average over all N bins and get the synchronization index

$$\lambda_{n,m} = N^{-1} \sum_{l=1}^{N} |\Lambda_l| \ . \tag{19}$$

According to the definition above $\lambda_{n,m}$ measures the conditional probability for ϕ_2 to have a certain value provided ϕ_1 is in a certain bin.

We compare now these three indices using the simulated data. As a first model example we take two coupled nonidentical Rössler oscillators (Eq. (10)); now we consider a noise free case. Increasing the coupling strength ε, we observe a transition to the synchronous state. This can be seen from Fig. 9a, where the difference of frequencies of two oscillators is plotted as a function of coupling strength. At $\varepsilon \approx 0.03$ this difference vanishes, i.e. synchronization occurs. The lower panel (Fig. 9b) shows the indices as functions of ε.

We see, that the indices are nonzero outside the synchronization region. It is not surprising: we have noted already that the distribution of the cyclic phase outside the region also has a peak. Thus, we can reveal the presence of interaction even if it is too weak to induce synchronization. Comparing the indices we can see that $\lambda_{1,1}$ and $\gamma_{1,1}$ are almost 1 inside the Arnold tongue, while the index $\rho_{1,1}$ attains essentially lower value; it has another drawback to be mentioned: the estimate of this index strongly depends on the number of bins used for computation of the histogram. The transition to the synchronous state appears to be more sharp if described by the indices $\gamma_{1,1}$ and $\rho_{1,1}$. We
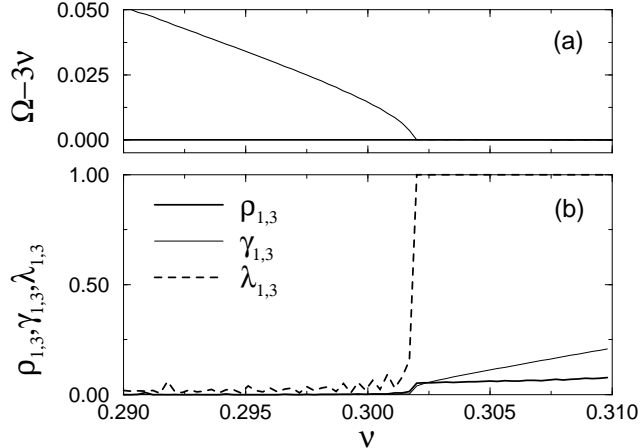
Fig. 10. Comparison of quantitative measures of synchronization using the simulated data from van der Pol oscillator with modulated natural frequency (Eq. (13)). Transition to synchronous state takes place when the difference of frequencies of two oscillators $\Omega - 3\nu$ vanishes with decrease of detuning (a). Three $1:3$ synchronization indices are shown as the functions of the frequency ν of the modulating force (b).

conclude, that if the goal of the analysis is to reveal very weak interaction then the conditional probability index $\lambda_{n,m}$ seems to be more appropriate. Alternatively, if we have a number of time series and try to sort them into groups - synchronized and not synchronized with respect to some reference signal - then the indices $\gamma_{n,m}$ and $\rho_{n,m}$ are more suitable.

As the second example we consider van der Pol oscillator with modulated natural frequency (Eq. 13). The distribution of the cyclic relative phase $\Psi_{1,3}$ is broad (cf. Fig. 6), and, thus, synchronization cannot be understood in terms of statistical phase locking. Therefore, the indices $\rho_{1,3}$ and $\gamma_{1,3}$ cannot reveal synchronization, while the conditional probability index $\lambda_{1,3}$ do indicates it (Fig. 10).

5.1   Human brain activity during pathological tremor

Motivation and experimental data

Here we briefly present the results of the investigation of phase synchronization between different brain areas, as well as between brain and muscle activity in Parkinsonian patients by means of noninvasive measurements [49,58]. These patients may exhibit involuntary shaking that is called tremor and predominantly affects the distal portion of the upper limb. Resting tremor in Parkinsonian patients has a principal frequency in the band $3 - 6$ Hz. The goal of the study was to find out whether synchronization between different cortical areas is involved in the generation of pathological tremor.

As is known, the neuronal activity of the human brain can be noninvasively assessed by registering the electric field with electroencephalography (EEG) [59], and the magnetic field with magnetoencephalography (MEG) [60–62]. The measurement of the magnetic field is realized by means of superconducting quantum interference devices (SQUIDs). An important advantage of MEG is that the scull and scalp are transparent to magnetic field. Therefore, in contrast to electric field, the externally measured magnetic field is not distorted. As a result of this, MEG allows to achieve a high spatial resolution and to distinguish between the cortical activity originating from distinct areas provided the latter are sufficiently remote.

The data were obtained by means of Neuromag-122 — a whole-head MEG systems consisting of 122 SQUIDs arranged in a helmet-shaped array [61]. In addition to the MEG, the electromyogram (EMG) from two antagonistic muscles exhibiting tremor activity, namely the right flexor digitorum superficialis muscle (RFM) and the right extensor indicis muscle (REM), was registered by standard techniques. The data are introduced in Fig. 11; from the power spectra one can see that they are not narrow-band signals. Therefore, filtration is required in order to separate the frequency band of interest from the background brain activity. The visual inspection of the data after preprocessing [6] shows that they are nonstationary.

Data analysis and results

The phase analysis was performed in the following way. First, the instantaneous phases of signals were obtained by means of the Hilbert transform. Next, one signal was taken as the reference one, and phase locking between this channel and all others was studied in pairs. To cope with nonstationarity, a sliding window analysis was done and the distribution of $\Psi_{n,m}$ was computed for every time point t within the window $[t - T/2, t + T/2]$ and characterized by means of the synchronization indices ρ and λ[7]. The window length T was varied between 2 and 20 s; the results are robust with respect to this variation. In search of *corticomuscular* synchronization (CMS), an EMG signal was taken as a reference signal. Investigation of *cortico-cortical synchronization*

---

[6] The EMG data were preprocessed in a standard way (cf. [63]) so that the resulting signal represents the time course of the muscular contraction. Then both EMG and MEG are band-pass filtered; the filter parameters are chosen in such a way that only the power around the main frequency, or around the main frequency and its second harmonics is preserved. The presented results correspond to the following parameters: bandpass of EMG signals: 5-7 Hz, bandpass of MEG signals: 5-7 and 10-14 Hz (for quantification of 1:1 and 1:2 locking, respectively). The results are robust with respect to variations of the band edges of all filters used; the usage of two-band filters (e.g., 5-7 Hz plus 10-14 Hz) produces consistent results.

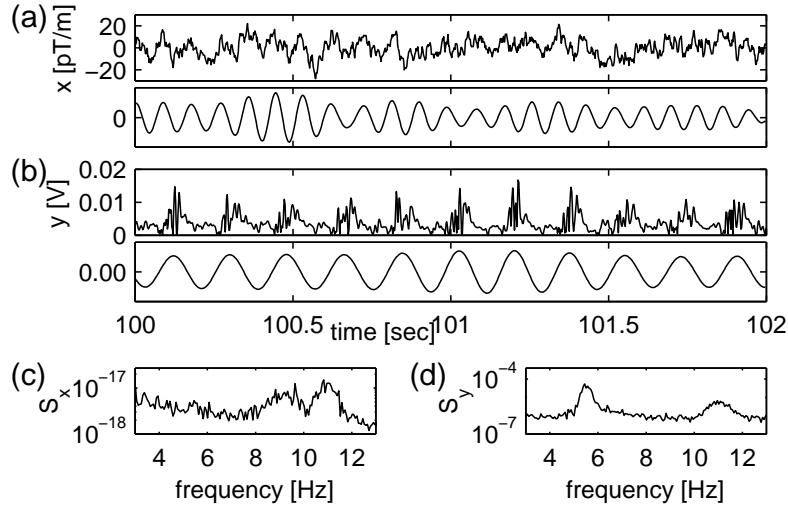[7] Computation of both indices gives consistent results.

Fig. 11. An original and filtered MEG signal (from a channel over the left sensorimotor cortex) (a) and its power spectrum (c). The original and preprocessed EMG signal of the right flexor digitorum muscle (b) and its power spectrum (d).

(CCS) was done by choosing for reference one of the MEG channels over the left sensorimotor cortex.

The main results are shown in Figs. 12,13. Pronounced tremor activity starts after ~ 50 s (Fig. 12a). It involves the coordinated activation and deactivation of flexor and extensor muscles that is reflected by antiphase locking of their EMG activity (Fig. 12b). This pereferal coordination may be a consequence of CMS or/and CCS — that is actually the hypothesis we are testing. Therefore, it is convenient to use the synchronization measures for characterization of the time course of the tremor activity. Then, one can verify whether this coordination reflects the time course of synchronization. Indeed, during the epoch of the significant tremor activity, corticomuscular as well as cortico-cortical synchronization were also observed. Namely, the activity of both sensorimotor cortex and premotor areas are 1 : 2 phase locked with the EMG activity of both flexor and extensor muscles (Figs. 12c and 13), whereas the activities of these two brain areas are 1 : 1 locked (Fig. 12d). It is important, that when the strength of peripheral coordination decreases during the last ~ 50 s, the strength of CMS and CCS is also reduced. Another important observation is that the onset of CCS precedes initiation of the tremor. These results confirm the sequential activation of motor cortex and tremor bursts revealed by Volkmann et al. [63] [8] and, thus, support the hypothesis of a central oscillator responsible for the generation of the Parkinsonian tremor.

Moreover, the phase analysis allows to localize the brain areas with MEG activity phase locked to tremor activity from noninvasive measurements (Fig. 13).

---

[8] This conclusion is based on their MEG study, animal experiments and recordings during neurosurgery in Parkinsonian patients.
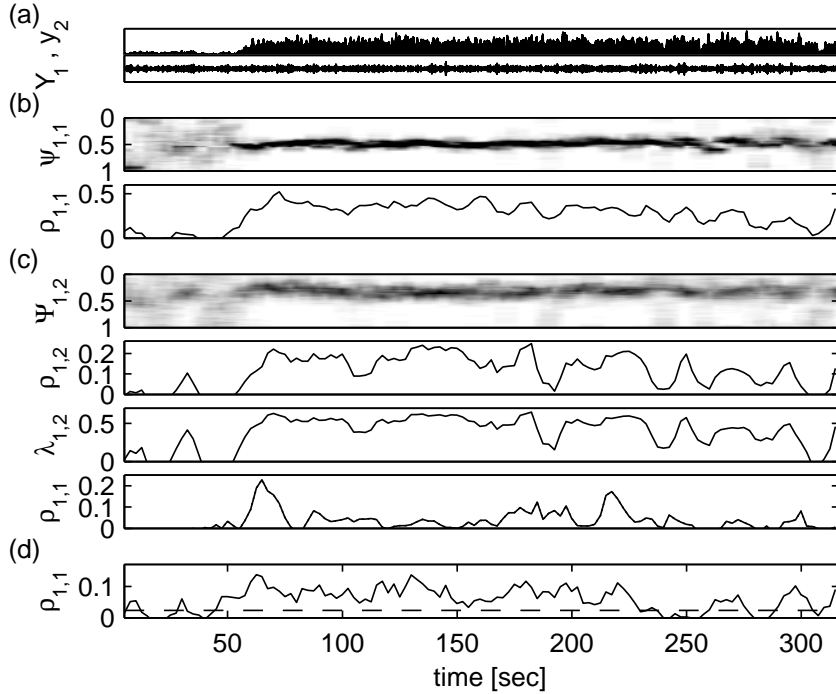
Fig. 12. (a): EMG of the right flexor muscle (RFM, upper trace) and an MEG over the left sensorimotor cortex (LSC) (lower trace). (b) 1 : 1 coordination between right flexor and extensor muscles: the distribution of the cyclic phase difference $\Psi_{1,1}$ computed in the running window $[t-5, t+5]$ is shown as a gray-scale plot, where white and black correspond to minimal and maximal values, respectively (upper plot); the lower plot shows the corresponding synchronization index $\rho_{1,1}$. (c) 1 : 2 corticomuscular synchronization: time course of the distribution of the cyclic phase difference $\Psi_{1,2}$ between MEG signal from the LSC and EMG of the RFM (uppermost plot) and of the corresponding indices $\rho_{1,2}$ and $\lambda_{1,2}$; for comparison, 1:1 synchronization index $\rho_{1,1}$ between LSC and RFM is shown below. (d) 1 : 1 cortico-cortical synchronization between LSC and a premotor MEG channel. Dashed line indicates the value of $\rho_{1,1}$ corresponding to 99.9th percentile of the surrogates (see Discussion).

The main focus of the 1 : 2 synchronization is located over the contralateral sensorimotor cortex. Additionally, this type of locking is observed over premotor, frontal, contralateral parietal and contralateral temporal areas. In contrast to the 1 : 2 locking, the 1 : 1 synchronization is much weaker, and is observed over contralateral sensorimotor, parieto-occipital and frontal areas. All areas which are 1 : 2 locked with the tremor are also 1 : 1 locked among each other.
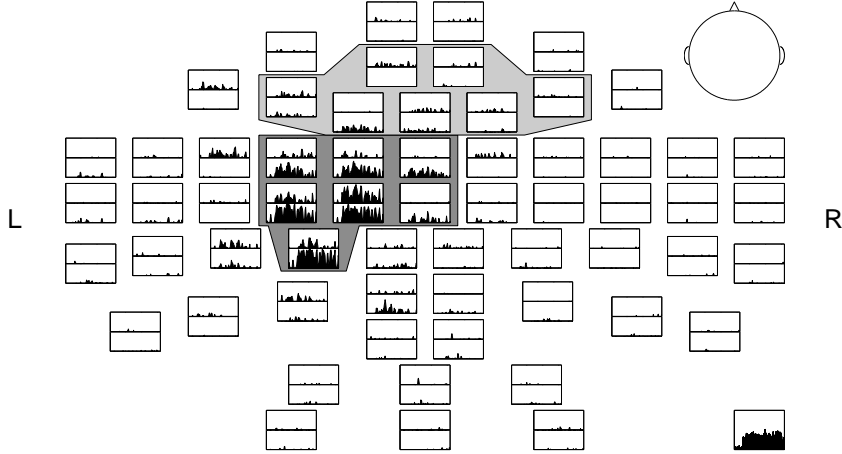
26

Fig. 13. Time dependence of the synchronization index $\rho_{1,2}$ characterizing $1 : 2$ locking between the EMG of the right flexor muscle (reference channel, plotted in the lower right corner) and all MEG channels. Each rectangle corresponds to an MEG sensor; time axis spans 310 s and y-axis scales from 0 to 0.25. The head is viewed from above, 'L' and 'R' mean left and right (see the "head" in the upper right corner). The upper and lower gray regions corresponds to premotor and contralateral sensorimotor areas respectively. The results are similar for the extensor muscle.

6 Stroboscopic technique: Application to cardiorespiratory interaction

In this Section we present the synchronization analysis of cardiorespiratory interaction in humans. The data we analyse, namely electrocardiogram (ECG) and respiratory signal, were already introduced in Fig. 4. The complexity of this case is related to the following features:

- the time series have essentially different forms (respiration is a narrow-band signal, while ECG can be reduced to the spike train);
- the characteristic time scales of two signals are different (there are always several heartbeats per respiratory cycle) and vary essentially within one experimental record; therefore we expect (and we indeed observe it) synchronization of some high order $n : m$ and transitions between different synchronous states;
- synchronization is probably related to modulation of the heartrate by respiration, so that stroboscopic methods suitable for the detection of $n : m$ locking from nonstationary data are required.

These features make the problem a very useful example for comparison of different analysis techniques.

27

6.1 Cardiorespiratory interaction

The human cardiovascular and respiratory systems do not act independently; their interrelation is rather complex and still remains a subject of physiological research (see, e.g. [20,64] and references therein). As a result of this interaction, in healthy subjects the heart rate normally increases during inspiration and decreases during expiration, i.e., the heart rate is modulated by a respiratory related rhythm. This frequency modulation of the heart rhythm (see Fig. 14) is known for at least a century and is commonly referred to as "respiratory sinus arrhythmia" (RSA). It is a well-studied phenomenon, see, e.g. [65–67].
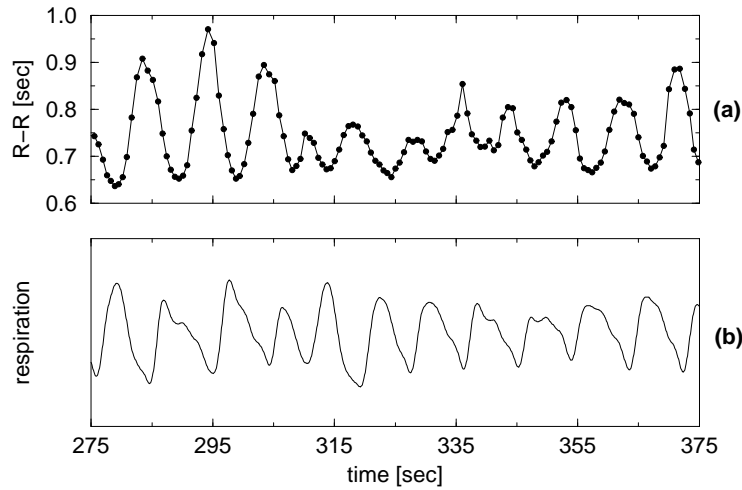

Fig. 14. An example of pronounced respiratory sinus arrhythmia: the heart rate (a) is modulated by a respiratory related rhythm. The respiratory signal (arbitrary units) is shown in (b).

The interaction between the cardiovascular system and respiration involves a large number of feedback and feed-forward mechanisms with different characteristic time scales. Definitely, it cannot be simply viewed at as unidirectional modulating action of respiration on the cardiovascular signal. Nevertheless, this modulation (RSA) is almost always observed in the data and therefore should be accounted for.

6.2 The experimental data and preprocessing

Here we report the results by Schäfer et al. [29,30], where the examinations with 8 healthy volunteers (14 to 17 years, high performance swimmers, 4 male, 4 female) were performed. The subjects were laying at rest and no constraints like paced respiration or mental exercising were used.

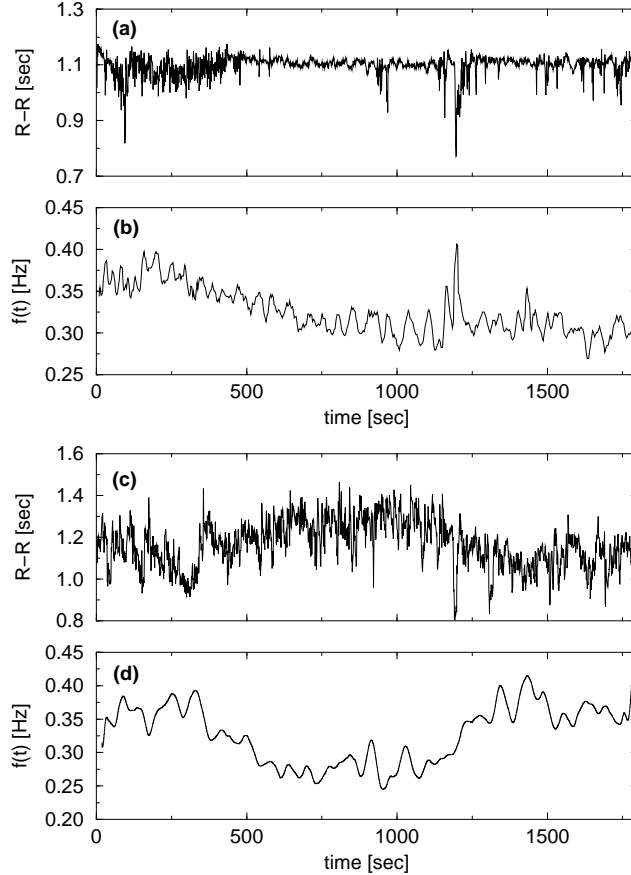The electrocardiogram (ECG) was registered by standard leads and respi-

Fig. 15. The data for subject A: time course of R-R (interbeat) intervals (a) and of the instantaneous frequency $f(t)$ of respiration (b) clearly demonstrate the non-stationarity of the time series. Similar data for subject B are shown in (c) and (d).

ration was measured simultaneously by a thermistor at the nose, while respiratory abdominal movements were registered for control. The duration of each record is 30 minutes. All signals were digitized with 1000 Hz sampling rate and 12 bit resolution. For the analysis of the heart rate the times of R-peaks in the ECG (Fig. 4a) were extracted by a semi-automatic algorithm with manual correction. Only data sets without extrasystoles were used for the subsequent analysis. The respiratory signals were visually inspected and, if required, preprocessed. After low-frequency trend elimination, a second-order Savitzky-Golay filter [68] was applied to remove high frequency noise.

Here we describe two representative data sets (Subjects A and B); the data used for the analysis are shown in Figs. 15. We note that subject B exhibits essentially more pronounced RSA: the average amplitude of the modulation is ≈ 4 times larger than that for subject A.

6.3 Cardiorespiratory synchrogram

First we present a graphic tool based on the stroboscopic technique. Here we use the phase stroboscope and observe the phase of the one oscillators at the instants of time when the phase of the second one attains a certain value. For the study of cardiorespiratory interaction the natural way is to make use of the fact, that ECG can be reduced to a point process. Hence, we observe the phase of the respiratory signal ϕ_r at the times t_k of appearance of k-th R-peak, and plot this phase versus t_k. In the noise-free case of $n : 1$ synchronization, we would observe n distinct values of the respiratory phase so that such a plot would exhibit n horizontal lines. Noise smears out these lines, and some bands are expected to be observed instead. To look for $n : m$ locking we use the wrapping of the respiratory phase into $[0, 2\pi m]$ interval, i.e. consider m adjacent oscillations as one cycle, and plot

$$\psi_m(t_k) = \frac{1}{2\pi}(\phi_r(t_k) \bmod 2\pi m) \tag{20}$$

versus t_k; we refer to this plot as *cardiorespiratory synchrogram* [29], see Fig. 16.

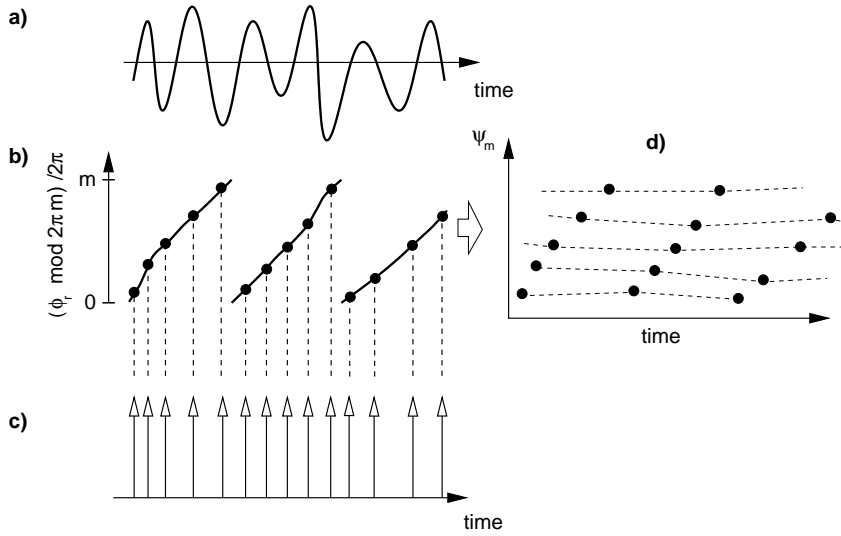Fig. 16. Principle of the phase stroboscope, or synchrogram. Here a slow signal (a) is observed in accordance with the phase of a fast signal (c). Measured at these instants, the phase of the slow signal wrapped modulo $2\pi m$, (i.e., m adjacent cycles are taken as a one longer cycle) is plotted in (d); here $m = 2$. In this presentation $n : m$ phase synchronization shows up as n nearly horizontal lines in (d).

An important feature of this graphic tool is that, in contrast to the phase difference plots, only one integer parameter m has to be chosen by trial. Moreover, several synchronous regimes can be revealed within one plot, and the transitions between them can be traced. Indeed, if due to nonstationarity the

30

coupled systems exhibit a transition from, e.g. $3:1$ to $5:2$ locking, then this is reflected in the proposed presentation with $m = 2$ as a transition from a 6- to a 5-line structure.

A very important property of the synchrogram is that it is equally effective in both cases of synchronization either by external or parametric forcing [30], see Fig. 17.
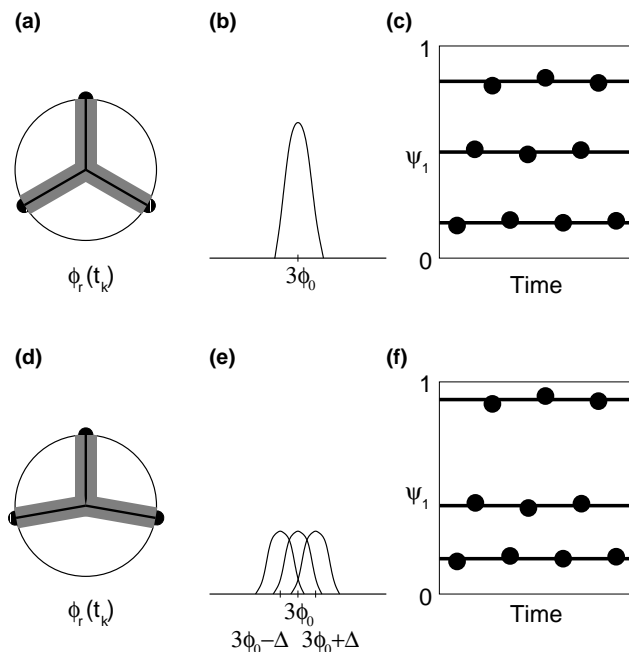

Fig. 17. Different efficiency of straightforward analysis of the relative phase and synchrogram technique in the case of synchronization via external forcing (a,b,c) and modulation (d,e,f); $3:1$ locking is taken here as an example. In the first case point events ("heartbeats") occur at three equally spaced values of the ("respiratory") phase. These values are shown by black points on the circle (a) and the corresponding radii. The noise smears these values, this is illustrated by the gray band around the radii. In this case, the distribution of the cyclic relative phase shows a single maximum (b). In the case of modulation, the events are not equally distributed on the circle (d) and the respective distribution (e) has three maxima and is essentially broader than the one shown in (b). As a result, the synchronization seems to be not well-expressed. Nevertheless, the synchrograms (c) and (f) efficiently reveal synchronization in both cases. The difference between synchronization via external forcing or modulation shows up by different distances between the horizontal bands in these plots.

Example of phase locking: subject A

The sequence of R-R intervals and frequency of respiration for subject A are presented in Fig. 15; nonstationarity is the essential feature of the data. First

31

we analyze the generalized phase difference $\varphi_{n,m}$ for different values n and m (Fig. 18), as well as instantaneous frequency ratio (not shown). The latter indicates the possibility of $5 : 2$ locking within the first ≈ 300s and of $3 : 1$ locking appearing after ≈ 750s[9]. From the analysis of relative phase only, we cannot reliably confirm the occurrence of synchronized epochs. Indeed, $\varphi_{3,1}$ exhibits some plateaus interrupted by phase slips only for the last 400s (see inlet in Fig. 18); $\varphi_{5,2}$, as well as the values of relative phase for other locking ratios, displays no plateaus in this presentation.
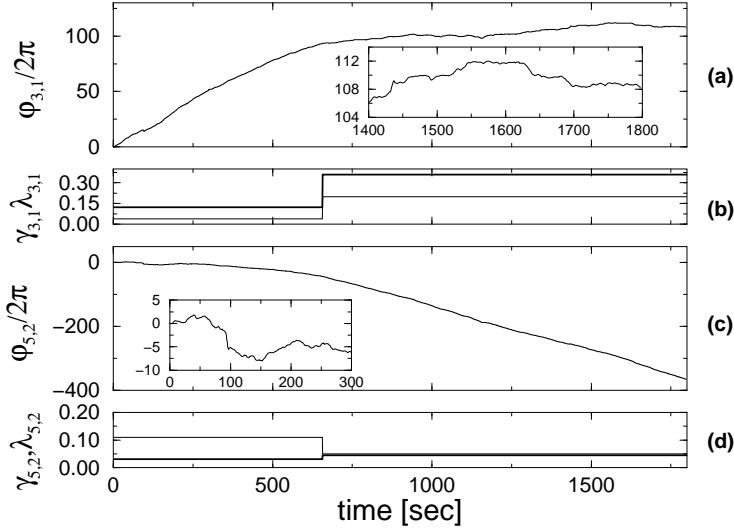

Fig. 18. Generalized phase difference and frequency ratio for subject A. Relative phase $\varphi_{3,1}$ (a) shows some indication for $3 : 1$ phase locking. For a comparatively short period of time one can see plateaus in the plot of $\varphi_{3,1}$ vs. time, interrupted by phase slips (see inlet). The indication for the locking is confirmed by synchronization indices $\gamma_{3,1}$ and $\lambda_{3,1}$ shown in (b) by bold and solid line, respectively. The time dependence of $\varphi_{5,2}$ (c) remains approximately constant during first 300s but displays no distinct plateaus, as can be seen from the zoomed plot (inlet). Nevertheless, the index $\lambda_{5,2}$ indicates some level of synchronization (d), solid line, while the index $\gamma_{5,2}$ (bold line) is practically zero.

The presence of $3 : 1$ locking becomes more evident if we analyse the phase difference statistically, i.e. consider the distribution of the cyclic relative phase $\Psi_{3,1}$ (cf. Eq. (8)). As the data are nonstationary, we compute this distribution in a running window (Fig. 19); the preference of a certain value of $\Psi_{3,1}$ within the last ≈ 900s is clearly seen.

Computation of synchronization indices $\gamma_{n,m}$ and $\lambda_{n,m}$ confirms the phase

---

[9] As the precision of computation of instantaneous frequencies in case of noisy data is rather poor, this method can be considered only as an auxiliary one. Its advantage is that there is no need to search for appropriate values of n and m, moreover, an approximately constant value of the ratio can be used for estimation of these integers.
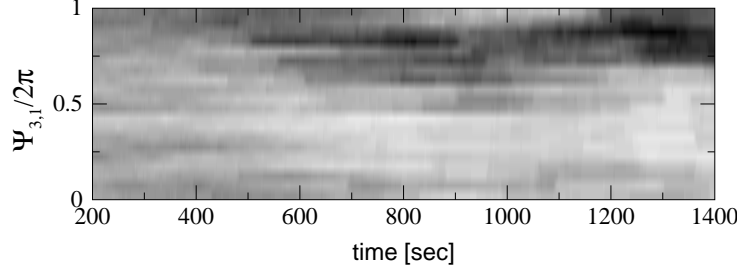
Fig. 19. Distribution of the cyclic relative phase $\Psi_{3,1}/2\pi$ calculated in a running window (400 heartbeats) and coded by gray scales also gives some indication of synchronization in the time interval 600 – 1400s. Black color corresponds to the maximal values.

locking. We note that for the 3 : 1 locking both indices give similar results, whereas the 5 : 2 locking within the first part of the records is indicated by the conditional probability index only.
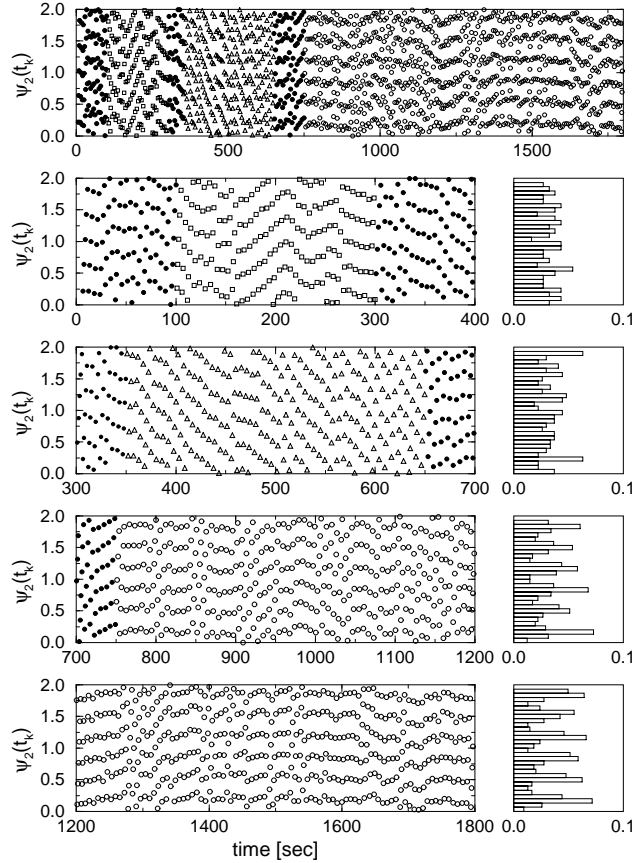

Fig. 20. (a) Cardiorespiratory synchrogram (CRS) of subject A, showing the transition from a five-band structure (5 : 2 locking) to a six-band structure (3 : 1 locking).

The next step is to perform the stroboscopic analysis of the respiratory phases as described in. The cardiorespiratory synchrogram (CRS) clearly exhibits 6 horizontal lines within the last ≈ 1000s (Fig. 20); this is confirmed by the respective distribution (phase density histogram) showing 6 well-expressed

33

peaks. This presentation makes the presence of the $3 : 1$ phase locking in the data quite evident.

Example of frequency locking: subject B

Within the first ≈ 300s the CRS for subject A (Fig. 20) has a clear 5-band structure. These bands are not horizontal, hence the distribution of ψ_2 is practically uniform, so that we cannot speak of phase locking. Nevertheless, the occurrence of these bands shows that, on average, two adjacent respiratory cycles contain 5 heartbeats; this may be considered as an indication of frequency locking. This indication is also supported by the conditional probability index $\lambda_{5,2}$ (Fig. 18d).
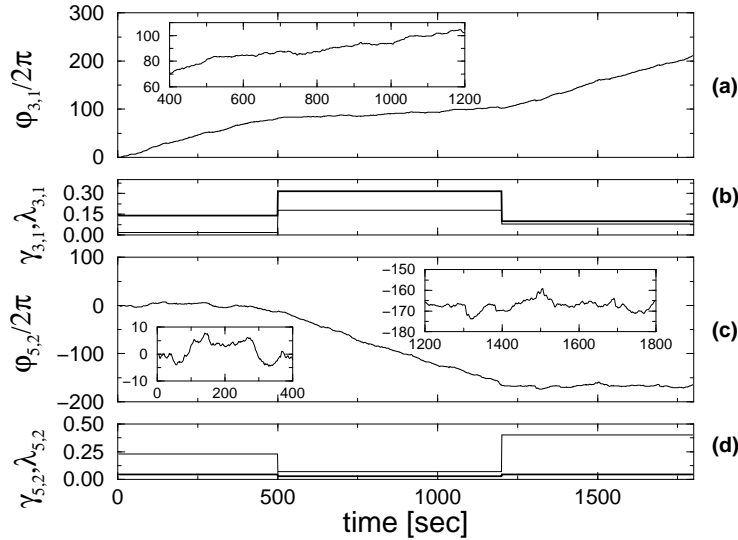

Fig. 21. Subject B. Relative phases $\varphi_{3,1}$ (a) and $\varphi_{5,2}$ (c) show some indication of $3 : 1$ and $5 : 2$ synchronization, respectively. This is consistent with the values of synchronization indices (b) and (d). Although the plateaus in the time course of the relative phase are not very distinct (see inlets in (a) and (b)), statistically understood $3 : 1$ phase locking can be confirmed by means of CRS (see Fig. 22). Note that within the last 600s the generalized phase difference fluctuates around a constant level, indicating frequency locking on average; this indication is supported by a high value of the conditional probability index $\lambda_{5,2}$.

Another illustrative example can be found in the data of subject B; these data were already introduced in Fig. 15b. The analysis of relative phase and synchronization indices (Fig. 21) indicates epochs of $3 : 1$ and $5 : 2$ synchronization. The CRS plot confirms that we encounter statistical $3 : 1$ phase locking within the time interval $\approx 400 - 1200$s (Fig. 22). The interval $1200 - 1800$s represents frequency locking; the relative phase $\varphi_{5,2}$ fluctuates around a constant value, so that on average the frequency ratio $f_h/f_r = 5 : 2$. Although we can
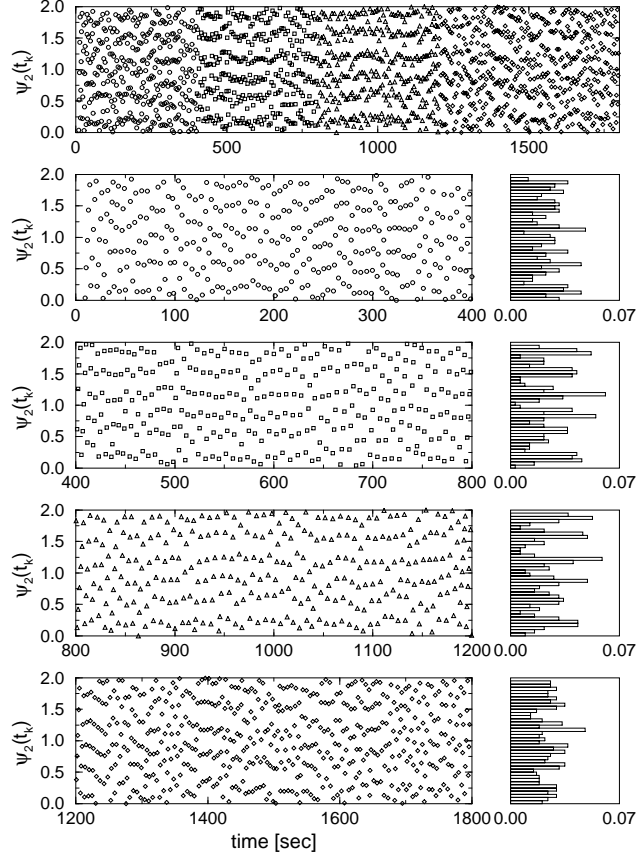
Fig. 22. (a) Cardiorespiratory synchrogram (CRS) of subject B demonstrates 6-band structure in the range 400–1200s confirming 3 : 1 phase locking. Note that there is no phase locking in the statistical sense in those intervals where the generalized phase difference (Fig. 21c) indicates 5 : 2 phase locking.

find some short epochs with 5 distinct bands (e.g. around $t = 1400$s), and the distribution of ψ_2 is not uniform, we cannot with confidence speak of phase locking in this case. From the other side, long lasting coincidence of frequencies by pure chance seems to be very unlikely. This regime probably arises due to dominating role of modulating influence of respiration on the heartrate (cf. model example Eq. (13)). We remind, that subject B has considerably higher RSA than subject A.

7 Discussion

7.1 Is it really synchronization?

An important issue is interpretation of the results of the phase analysis. Here we have to be aware of two problems:

- Can we be sure that the patterns of the relative phase, described in the sections above, indeed indicate synchronization, and, respectively, underlying nonlinear dynamics?
- How reliable is this indication?

Before we address these questions, we remind that the synchronization transition in noisy systems is smeared. Next, as we already stressed, the relation between phases indicates, strictly speaking, the presence of interaction between systems, but not necessarily means that they are synchronized. Finally, our synchronization approach to data analysis is based on certain assumptions that might be not always fulfilled. All in all, we can never unambiguously state that we have observed synchronization; nevertheless, strong indications in favour of such a conclusion can be sometimes found.

As synchronization is not *a state, but a process* of adjustment of rhythms due to interaction, we cannot validate its existence if we do not have access to the system parameters and cannot check experimentally that the synchronous state is stable towards variation of the parameter mismatch within a certain range (i.e. if we cannot plot the frequency vs. detuning curve). If we are not able to do such experiments, but just have some data sets registered under free-running conditions, the only way to get some confirmation (but certainly not a proof) on the existence of synchronization is to make use of the fact that the data are nonstationary. Indeed, we can trace the variation of the instantaneous frequencies of both signals and their relation with time. If we find some epochs, as in the case of cardiac and respiratory data, where both frequencies vary, but their relation remains stable (Fig. 23), this can be considered as a strong indication in favor of our conclusion.

Another indication that also can be obtained using the fact of nonstationarity of the data is the presence of several different $n : m$ epochs within one record. Indeed, one can argue that observed phase or frequency locking of, e.g. order $3 : 1$, could be due to the coincidence of frequencies of the uncoupled systems. Nevertheless, occasional coincidence of frequencies having the ratios exactly corresponding to neighboring Arnold tongues seems to be very unlikely.

If the data are rather stationary and we are not able to find such epochs, the situation is more difficult. Suppose that the distribution of the relative phase
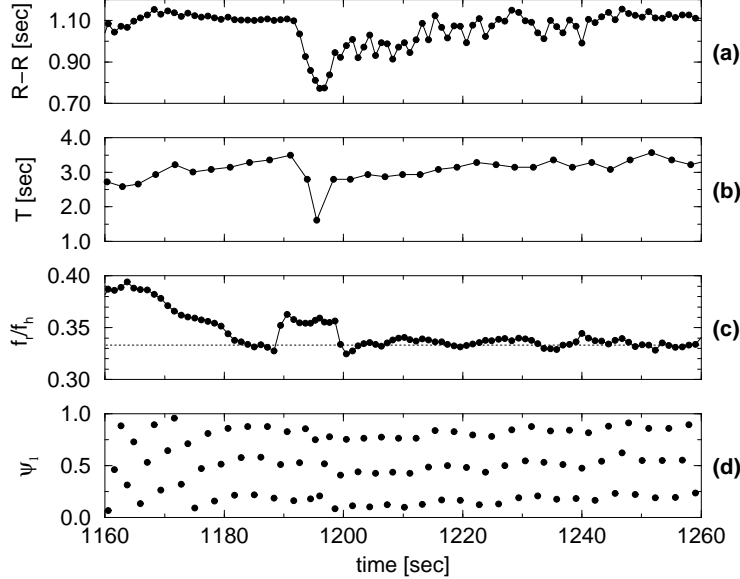
Fig. 23. A transient epoch within the data of subject A confirms the existence of synchronization. The periods of cardiac (R-R) and respiratory cycles (T) are shown in (a) and (b), respectively. After a short epoch of non-synchronous behavior (1150–1200s) the frequencies of heart rate and respiration change, probably due to influence of a certain control mechanism, and become locked, i.e., $f_r/f_h \approx 1/3$. In the next 50s we observe that, although both frequencies decrease, this ratio remains almost constant (c). This means that one of the systems follows the other one, i.e., synchronization takes place. $3:1$ phase locking is also clearly seen from CRS (d).

for such a bivariate record is non-uniform. Can it just happen due to an occasional coincidence of frequencies? From the theory and the simulation of the model example (Eq. (10)) we know that even if the frequencies of uncoupled oscillators are equal, the distribution of $\Psi_{n,m}$, computed on a sufficiently long time scale, has to be nearly uniform due to the diffusion of the phase. Certainly, occasionally one can find short epochs where phases seem to be locked. How can we estimate what is "short" and "long" in this context?

From the first sight, a natural way to address this problem is to use the surrogate data techniques [69,28]. However, we see some serious problems in this approach. The usual formulation of the null hypothesis that is used for nonlinearity tests is to consider a Gaussian linear process [70,71] with a power spectrum that is identical to that of the tested signal; more sophisticated methods [72] imply also preservation of the probability distribution. A modification of this null hypothesis for the tests for synchronization — a consideration of two surrogate signals that preserve the linear cross-correlation between the original data — seems to be not sufficient. Indeed, due to the definition of synchronization, we are interested in the relation between instantaneous phases, whereas the variations of amplitudes and their interrelation are of no importance. The usual way to construct surrogates (the randomization of Fourier phases) *mixes the phase and amplitude properties*, transforming the variation

37

of instantaneous phase into the variation of instantaneous amplitude and vice versa. Moreover, the signals generated by self-sustained oscillators possess certain properties of the distribution of instantaneous amplitudes (see [73] and references therein), and this distribution is destroyed by the Fourier phase randomization.

Although we cannot give a general recipe how to estimate the reliability of phase analysis, some empirical methods can be used in particular experiments. So, in the above described MEG study [49,49] the surrogates were constructed by taking either white noise or empty room measurements (instrumental noise) and filtering them with the same band-pass filter as the data. The 95th percentile of the distribution of a synchronization index for surrogates was taken as the significance level. Afterwards, the synchronization indices were re-calculated in accordance to this level, e.g. $\rho_{n,m} \to \max\{\rho_{n,m} - \tilde{\rho}, 0\}$, where $\tilde{\rho}$ is the significance level.

7.2 Synchronization versus coherence

Very important question is the relation of the synchronization analysis to the cross-spectrum techniques (coherence estimates) and to mutual information approach that are widely used, e.g. for the analysis of brain activity [74–76]. This problem requires a systematic study for different types of coupling; here we present only preliminary results.

First, we mention that synchronization is not equivalent to correlation (coherence). Indeed, if two systems synchronize, their signals are correlated. On the contrary, coherence does not necesserely show the presence of synchronization; it may be for example caused by mixing of signals (see Fig. 1). This scheme imitates the real situation: e.g., each MEG sensor measures signals originating from more than one area of neuronal activity. To simulate this, we construct artificial signals $u = (1 - \mu)x_1 + \mu x_2$ and $w = \mu x_1 + (1 - \mu)x_2$; where x_1 and x_2 are the solutions of Eq. (10) for the parameters $D = 0.2$, $\mu = 0.02$ and $\varepsilon = 0$, i.e. they are the outputs of two *uncoupled Rössler* oscillators. This mixture of signals does not lead to a spurious detection of synchronization, i.e. the relative phase is not bounded, although u and w are correlated: the cross-spectrum analysis by means of the Welch technique with the Bartlett window indeed reveals significant coherence $\gamma^2 = 0.43$.

The difference between the results of phase analysis and coherence can be also demonstrated with real data. In Fig. 24 we present the results of cross-spectrum analysis of all the MEG channels and the reference channel that was the EMG of the flexor muscle. Each rectangle in the plot shows the coherence between the respective MEG channel and the reference one. Contralateral

sensorimotor MEG signals are coherent with EMG, in accordance with the concepts known in neuroscience [63]. Nevertheless, one can also see tremor coherent MEG activity extended over the right hemisphere in contradiction to this concept. Insufficiency of the coherence technique can additionally be seen from the fact that MEG channels overlying sensorimotor and premotor areas are coherent with practically all other MEG channels. Comparing Fig. 24 with the results of the synchronization analysis (Fig. 13) we conclude that the latter technique allows better localization of the tremor related brain activity.
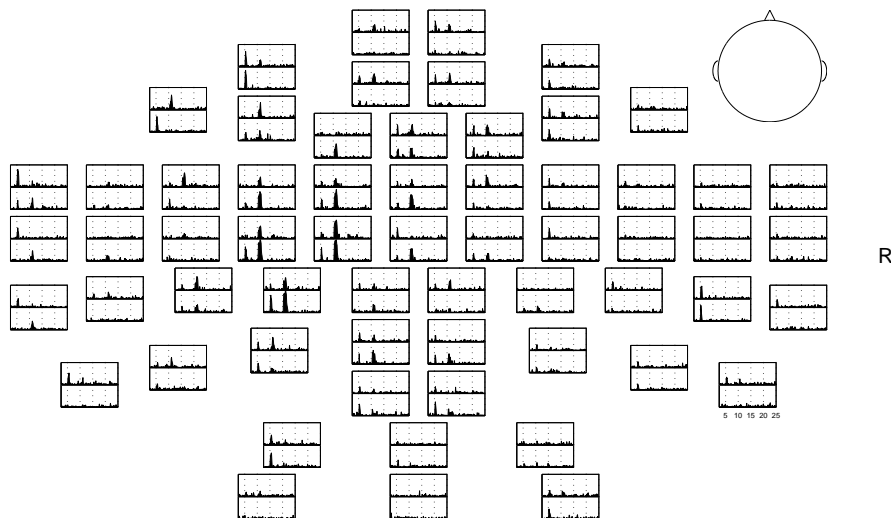

Fig. 24. Results of the cross-spectrum analysis between EMG of the right flexor muscle (reference channel) and all MEG channels. The coherence function γ^2 is plotted vs. frequency. Each rectangle corresponds to an MEG sensor; the x-axis spans 2.5 to 25 Hz and y-axis scales from 0 to 0.75.

8   Appendix: Instantaneous phase and frequency of a signal

8.1   Analytic signal and the Hilbert Transform

A consistent way to define the phase of an *arbitrary signal* is known in signal processing as the analytic signal concept [77,40,78,79]. This general approach, based on the Hilbert transform (HT) and originally introduced by Gabor in

1946 [52], unambiguously gives the *instantaneous phase and amplitude* for a signal $s(t)$ via construction of the *analytic signal* $\zeta(t)$, which is a complex function of time defined as

$$\zeta(t) = s(t) + \imath s_H(t) = A(t)e^{\imath \phi(t)} \,, \tag{21}$$

where the function $s_H(t)$ is the HT of $s(t)$

$$s_H(t) = \pi^{-1}\text{P.V.} \int\limits_{-\infty}^{\infty} \frac{s(\tau)}{t - \tau} d\tau \,, \tag{22}$$

and P.V. means that the integral is taken in the sense of the Cauchy principal value. The instantaneous amplitude $A(t)$ and the instantaneous phase $\phi(t)$ of the signal $s(t)$ are thus uniquely defined from (21). We note, that HT is parameters free.

As one can see from (22), the HT can be considered as the convolution of the functions $s(t)$ and $1/\pi t$. Due to the properties of convolution, the Fourier transform $S_H(\omega)$ of $s_H(t)$ is the product of the Fourier transforms of $s(t)$ and $1/\pi t$. For physically relevant frequencies $\omega > 0$, $S_H(\omega) = -\imath S(\omega)$. This means that the Hilbert transform can be realized by an ideal filter whose amplitude response is unity, and the phase response is a constant $\pi/2$ lag at all frequencies.

Although formally $A(t)$ and $\phi(t)$ can be obtained for an arbitrary $s(t)$, they have clear physical meaning only if $s(t)$ is a narrow-band signal, see the detailed discussion in [79]. For narrow-band signals the amplitude $A(t)$ coincides with the envelope of $s(t)$, and the *instantaneous frequency* corresponds to the frequency of the maximum in the instantaneous spectrum.

We illustrate the properties of the Hilbert transform by the following examples.

Example 1: Damped oscillations.   Let us take as the measured signals free oscillations of linear

$$\ddot{x} + 0.05\dot{x} + x = 0 \tag{23}$$

and Duffing

$$\ddot{x} + 0.05\dot{x} + x + x^3 = 0 \tag{24}$$

oscillators, and calculate from $x(t)$ instantaneous amplitudes $A(t)$ and frequencies $d\phi/dt$ (Fig. 25). The amplitudes, shown as thick lines, are really envelopes
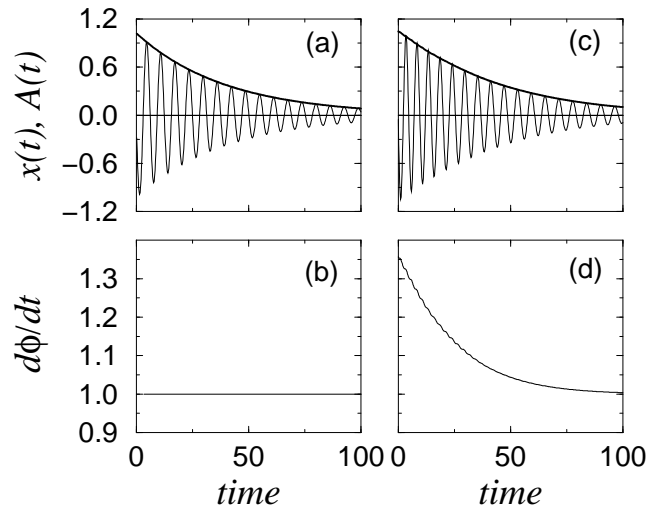
Fig. 25. Free vibrations $x(t)$ of the linear (a) and nonlinear (Duffing) (c) oscillators. The instantaneous amplitudes $A(t)$ calculated via Hilbert transform are shown by thick lines. Corresponding instantaneous frequencies $d\phi/dt$ are shown in (b) and (d).

of the decaying processes. The frequency of the linear oscillator is constant, while frequency of the Duffing oscillator is amplitude-dependent, as expected. Note, that although only about 20 periods of oscillations have been used, the nonlinear properties of the system can be easily seen from the time series, because frequency and amplitude are estimated in every point of the signal. This method is used in mechanical engineering for identification of elastic and damping properties of a vibrating system [80]. This example illustrate the important property of the HT: it can be applied to nonstationary data.

Example 2: A chaotic signal. HT can be considered as a two-dimensional embedding in coordinates s, s_H. Let us choose as an observable the x coordinate of the Rössler system. The phase portrait of this system in coordinates x, x_H is shown in Fig.26; one can see that it us very similar to the "true" portrait of the Rössler oscillator in coordinates x, y. Instantaneous amplitude and phase are shown in Fig. 27. The phase ϕ grows practically linear, nevertheless small irregular fluctuations of that growth are seen. This agrees with the known fact that oscillations of the system are chaotic, but the power spectrum of $x(t)$ contains a very sharp peak.

Example 3: Human electrocardiogram. As an example of a complex signal we take a human ECG record (Fig. 28). We see that the point in the s, s_H-plane makes two rotations corresponding to the so-called R and T-waves, respectively. (Small loops corresponding to the P-waves are not seen in this magnification.) What is important, the trajectories in s, s_H pass through the origin, and therefore the phase is not always defined. We did not encounter
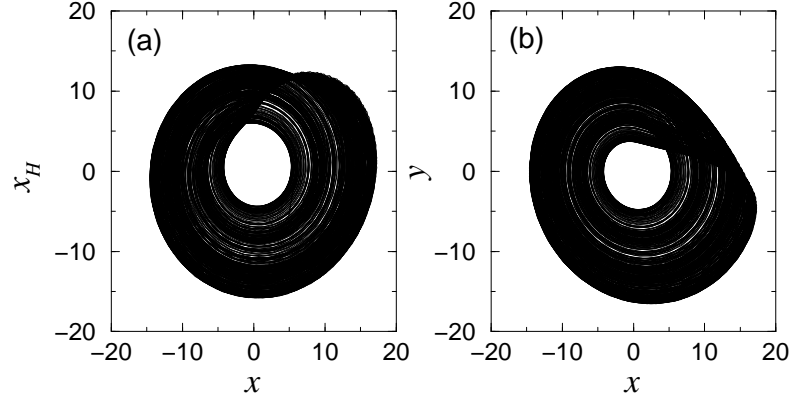
41

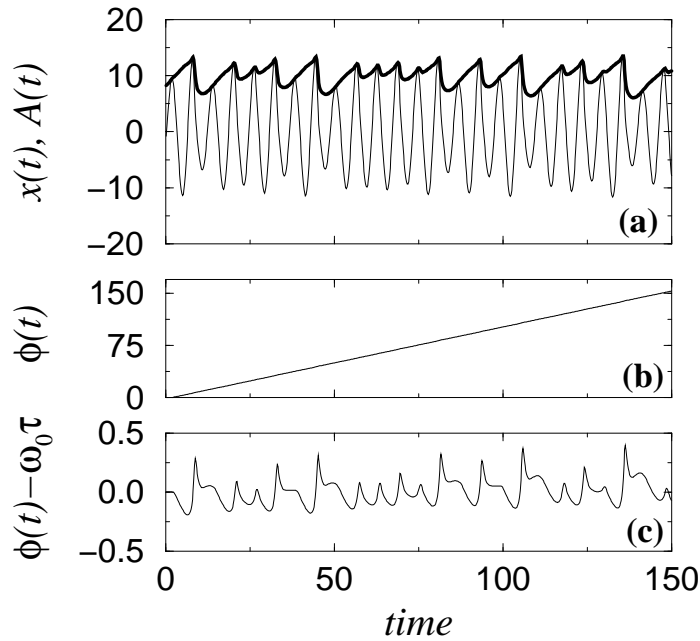Fig. 26. Phase portrait of the Rössler system in $x - x_H$ coordinates.

Fig. 27. Solution of the Rössler system $x(t)$ and its instantaneous amplitude $A(t)$ (thick line) (a). Instantaneous phase ϕ grows practically linear (b), nevertheless small irregular fluctuations are seen (c).

this problem in the previous examples, because of the simple structure of the signals there. Indeed, the normal procedure before computing the HT is to subtract the mean value from the signal. Often this ensures that trajectories go around the origin; we implicitly used this fact before. In order to compute the phase for the cardiogram, we have to transfer the origin to the point s^*, s_H^* and compute the phase as

$$\phi = \arctan\left(\frac{s - s^*}{s_H - s_H^*}\right) . \tag{25}$$

42

Definitely, in this way we loose the unambiguity in the determination of phase: now it depends on the choice of the origin. Two reasonable choices are shown in (Fig. 28c) by two arrows. Obviously, depending on the new origin in this plane, one cardiocycle (interval between two heartbeats) would correspond to the phase increase of either 2π or 4π. This reflects the fact that our understanding of what is "one oscillation" depends on the particular problem and our physical intuition.
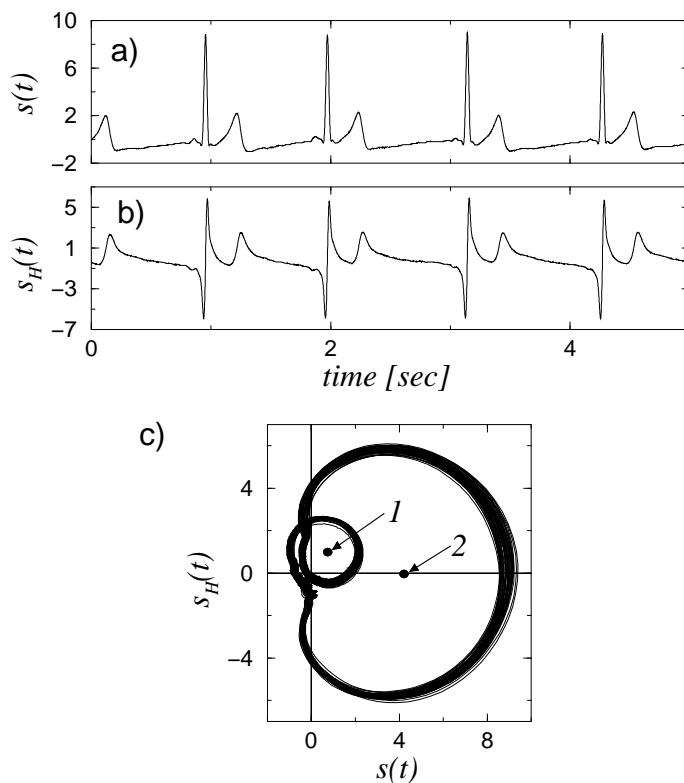

Fig. 28. Human ECG (a) and its Hilbert transform (b) and ECG vs its Hilbert transform (c). Determination of phase depends on the choice of the origin in the (s, s_H) plane; two reasonable choices are shown in (c) by two arrows.

8.2 Numerics: hints and know-hows

An important advantage of the analytic signal approach is that the instantaneous phase and the amplitude can be easily obtained from experimentally measured scalar time series.

Computing HT in the frequency domain. The easiest way to compute the HT is to perform the FFT of the original time series, shift the phase

of every frequency component by $-\pi/2$[10] and apply the inverse FFT. Zero padding should be used to make the length of the time series suitable for the FFT. To reduce the boundary effects, it is recommended to eliminate at least 10 quasiperiods at the beginning and the end of the signal. Such a computation with double precision allows to obtain the HT with the precision of about 1%. (The precision was estimated by computing the variance of $s(t) + H^2(s(t))$, where H^2 means that HT was performed twice; theoretically $s(t) + H^2(s(t)) \equiv 0$.)

Computing HT in the time domain. Numerically, this can be done via convolution of the experimental data with a pre-computed characteristic of the filter (Hilbert transformer) [40,78,81]. Such filters are implemented, e.g. in the software packages MATLAB [81] and RLAB (public domain, URL: http://www.eskimo.com/~ians/rlab.html). Although HT requires computation on the infinite time scale, i.e., the Hilbert transformer is an infinite impulse response filter, the acceptable precision of about 1% can be obtained with the 256-point filter characteristic. The sampling rate must be chosen in order to have at least 20 points per average period of oscillation. In the process of computation of the convolution $L/2$ points are lost at both ends of the time series, where L is the length of the transformer.

Computing and unwrapping phase. The convenient way to compute the phase is to use the functions `DATAN2`(s_H, s) (FORTRAN) or `atan2`(s_H, s) (C) that give the cyclic phase in the $[-\pi, \pi]$ interval. The relative phase, or phase difference of two signals $s_1(t)$ and $s_2(t)$, can be obtained via the Hilbert transform as

$$\phi_1(t) - \phi_2(t) = \arctan \frac{s_{H,1}(t)s_2(t) - s_1(t)s_{H,2}(t)}{s_1(t)s_2(t) + s_{H,1}(t)s_{H,2}(t)} . \tag{26}$$

For the detection of synchronization it is usually necessary to use the phase that is defined not on the circle, but on the whole real line. For this purpose the phase (or relative phase) can be unwrapped by tracing the $\approx 2\pi$ jumps in the time course of $\phi(t)$.

Sensitivity to low-frequency trends. We discussed already that phase is well defined only if the trajectories in the s, s_H-plane always go around the origin. This may be violated if the signal contains low-frequency trends, e.g.

---

[10] This can be conveniently implemented by swapping the imaginary and real parts of the Fourier transform: $\mathrm{Re}(\omega_i) \to \mathrm{tmp}$, $\mathrm{Im}(\omega_i) \to \mathrm{Re}(\omega_i)$, -tmp $\to \mathrm{Im}(\omega_i)$, where tmp is some dummy variable.

due to the drift of the zero level of the measuring equipment. If, as the result, some trajectory misses the origin, this oscillation will not be counted as a cycle, and 2π will be lost in the overall increase of the phase. To illustrate it, we add an artificial trend to the ECG signal; the embedding of this signal in coordinates s, s_H is shown in Fig. 29, to be compared with the same presentation for the original data in Fig. 28. Obviously, the origin denoted in Fig. 28 by the first arrow would be in this case a wrong choice. To avoid these problems, we recommend always to plot the signal versus its HT and to check whether the origin is chosen correctly.
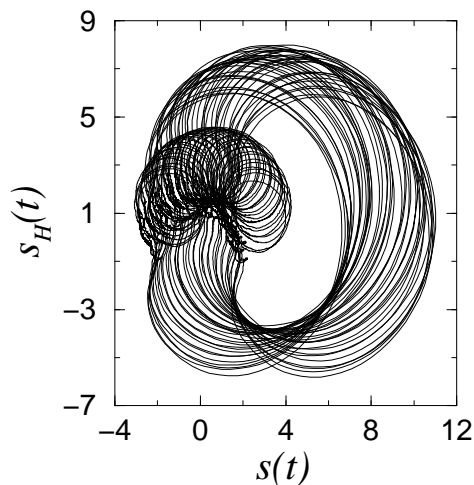

Fig. 29. An illustration of the sensitivity of the Hilbert transform to low-frequency trends.

Instantaneous frequency. We note, that estimation of instantaneous frequency $f(t)$ of a signal is rather cumbersome. Direct approach, i.e., numerical differentiation of $\phi(t)$, naturally results in very large fluctuations in the estimate of $f(t)$. Moreover, one may encounter that $f(t) < 0$. This happens not only due to the influence of noise, but can result from a complicated form of the signal. For example, some characteristic patterns in the ECG (e.g. the T-wave) result in negative values of instantaneous frequency. From a physical point of view, we expect that the instantaneous frequency is a positive function of time that varies slowly with respect to the characteristic period of oscillations and has a sense of a number of oscillations per time unit. This is especially important for the problem of synchronization where we are not interested in the behavior of the phase on a time scale smaller than the characteristic oscillation period. There exist several methods to obtain the estimates of $f(t)$ in accordance to this viewpoint; for a discussion and comparison see [79,30].

References

[1] Hugenii (Huygens), C. H. (1673) Horologium Oscillatorium (Apud F. Muguet, Parisiis, France; English translation: 1986, Iowa State University Press, Ames).

[2] Hayashi, C. (1964) Nonlinear Oscillations in Physical Systems (McGraw-Hill, New York).

[3] Blekhman, I. I. (1971) Synchronization of Dynamical Systems (Nauka, Moscow), (in Russian).

[4] Blekhman, I. I. (1981) Synchronization in Science and Technology (Nauka, Moscow, (in Russian); English translation: 1988, ASME Press, New York).

[5] Landa, P. (1996) Nonlinear Oscillations and Waves in Dynamical Systems (Kluwer Academic Publishers, Dordrecht–Boston–London).

[6] Fujisaka, H., and Yamada, T. (1983) Prog. Theor. Phys. **69**, 32–47.

[7] Pikovsky, A. S. (1984) Z. Physik B **55**, 149–154.

[8] Pecora, L. M., and Carroll, T. L. (1990) Phys. Rev. Lett. **64**, 821–824.

[9] Rosenblum, M., Pikovsky, A., and Kurths, J. (1996) Phys. Rev. Lett. **76**, 1804-1807.

[10] Pikovsky, A., Rosenblum, M., Osipov, G., and Kurths, J. (1997) Physica D **104**, 219–238.

[11] van der Pol, B., and van der Mark, J. (1928) Phil. Mag. **6**, 763–775.

[12] Aschoff, J., Daan, S., and Groos, G. (1982) Vertebrate Circadian Systems. Structure and Physiology (Springer, Berlin).

[13] Glass, L., and Mackey, M. C. (1988) From Clocks to Chaos: The Rhythms of Life (Princeton Univ. Press, Princeton, NJ).

[14] Petrillo, G. A., and Glass, L. (1984) Am. J. Physiol. **246**, 311–320.

[15] Bramble, D., and Carrier, D. (1983) Science **219**, 251–256.

[16] Collins, J., and Stewart, I. (1993) J. Nonlinear Sci. **3**, 349–392.

[17] Sturis, J., Knudsen, C., O'Meara, N. M., Thomsen, J. S., Mosekilde, E., VanCauter, E., and Polonsky, K. S. (1995), CHAOS **5**, 193–199.

[18] Neiman, A., Ping, X., Russel, D., Wojtenek, W., Wilkens, L., Moss, F., Braun, H., Huber, M., and Voigt, K. (1999) Phys. Rev. Lett. **82**, 660–663.

[19] Anishchenko, V. S., Balanov, A., Janson, N., Igosheva, N., and Bordyugov, G. (1999) Phys. Rev. Lett. (submitted).

[20] Koepchen, H. (1991) in: Rhythms in Physiological Systems, eds H. Haken and H. Koepchen, Vol. 55 of *Springer Series in Synergetics* (Springer, Berlin Heidelberg), pp. 3–20.

[21] Stutte, K., and Hildebrandt, G. (1966) Pflügers Arch. **289**, R47.

[22] Engel, P., Hildebrandt, G., and Scholz, H.-G. (1968) Pflügers Arch. **298**, 258–270.

[23] Pessenhofer, H., and Kenner, T. (1975) Pflügers Archiv **355**, 77–83.

[24] Kenner, T., Pessenhofer, H., and Schwaberger, G. (1976) Pflügers Arch. **363**, 263–265.

[25] Raschke, F. (1987) in: Temporal Disorder in Human Oscillatory Systems, eds L. Rensing, U. an der Heiden, and M. Mackey, Vol. 36 of *Springer Series in Synergetics*, (Springer, Berlin Heidelberg) pp. 152–158.

[26] Raschke, F. (1991) in: Rhythms in Physiological Systems, eds H. Haken and H. P. Koepchen, Vol. 55 of *Springer Series in Synergetics*, (Springer, Berlin Heidelberg) pp. 155 – 164.

[27] Schiek, M., Drepper, F., Engbert, R., Abel, H.-H., and Suder, K. (1998) Nonlinear Analysis of Physiological Data, eds H. Kantz, J. Kurths, and G. Mayer-Kress (Springer, Berlin) pp. 191–209.

[28] Seidel, H., and Herzel, H. (1998) IEEE Engineering in Medicine and Biology **17**, 54–57.

[29] Schäfer, C., Rosenblum, M. G., Kurths, J., and Abel, H.-H. (1998) Nature **392**, 239–240.

[30] Schäfer, C., Rosenblum, M., Abel, H.-H., and Kurths, J. (1999) Phys. Rev. E **60**, 857–870.

[31] Singer, W., and Gray, C. (1995) Annu. Rev. Neurosci. **18**, 555–586.

[32] Gray, C., and Singer, W. (1987) Soc. Neurosci. **404**, 3.

[33] Eckhorn, R., Bauer, R., Jordan, W., M.Brosch, Kruse, W., Munk, M., and Reitboeck, H. (1988) Biol. Cybern. **60**, 121–130.

[34] Gray, C., and Singer, W. (1989) Proc. Natl. Acad. Sci. USA **86**, 1698–1702.

[35] MacKay, W. (1997) Trends in Cognitive Sciences **1**, 176–183.

[36] Roelfsema, P., Engel, A., König, P., and Singer, W. (1997) Nature **385**, 157–161.

[37] Engel, J., and Pedley, T. (1975) Epilepsy : A Comprehensive Textbook (Lippincott-Raven, Philadelphia).

[38] Freund, H.-J. (1983) Physiological Reviews **63**, 387–436.

[39] Elble, R., and Koller, W. (1990) Tremor (John Hopkins University, Baltimore).

[40] Rabiner, L., and Gold, B. (1975) Theory and Application of Digital Signal Processing (Prentice–Hall, Englewood Cliffs, NJ).

[41] Rényi, A. (1970) Probability Theory (Akadémiai Kiadó, Budapest).

[42] Pompe, B. (1993) J. Stat. Phys. **73**, 587–610.

[43] Voss, H., and Kurths, J. (1997) Phys. Lett. A **234**, 336–344.

[44] Schiff, S., So, P., Chang, T., Burke, R., and Sauer, T. (1996) Phys. Rev. E **54**, 6708–6724.

[45] Pecora, L. M., Carroll, T. L., and Heagy, J. F. (1997) in: Nonlinear Dynamics and Time Series, eds C. D. Cutler and D. T. Kaplan, Vol. 11 of *Fields Inst. Communications* (American Math. Soc., Providence, Rhode Island), pp. 49–62.

[46] Rosenblum, M., Pikovsky, A., and Kurths, J. (1997) IEEE Trans. CAS-I **44**, 874–881.

[47] Rosenblum, M. G., and Kurths, J. (1998) in: Nonlinear Analysis of Physiological Data, eds H. Kantz, J. Kurths, and G. Mayer-Kress, (Springer, Berlin) pp. 91–99.

[48] Rosenblum, M. G., Firsov, G. I., Kuuz, R., and Pompe, B. (1998) in Nonlinear Analysis of Physiological Data, eds H. Kantz, J. Kurths, and G. Mayer-Kress, (Springer, Berlin), pp. 283–306.

[49] Tass, P., Rosenblum, M., Weule, J., Kurths, J., Pikovsky, A., Volkmann, J., Schnitzler, A., and Freund, H.-J. (1998) Phys. Rev. Lett. **81**, 3291–3294.

[50] Ott, E. (1992) Chaos in Dynamical Systems (Cambridge Univ. Press, Cambridge).

[51] Stratonovich, R. (1963) Topics in the Theory of Random Noise (Gordon and Breach, New York).

[52] Gabor, D. (1946) J. IEE London **93**, 429–457.

[53] Gurfinkel, V., Kots, Y., and Shik, M. (1965) Regulation of Posture in Humans (Nauka, Moscow).

[54] Cernacek, J. (1980) Agressologie **21D**, 25–29.

[55] Furman, J. (1994) in: Bailliére's Clinical Neurology, Vol. 3. (Bailliére Tindall) pp. 501–513.

[56] Lipp, M., and Longridge, N. (1994) J. of Otolaryngology **23**, 177–183.

[57] Otnes, R., and Enochson, L. (1972) Digital Time Series Analysis (John Wiley & Sons, New York).

[58] Tass, P., Kurths, J., Rosenblum, M., Weule, J., Pikovsky, A., Volkmann, J., Schnitzler, A., and Freund, H.-J. (1999) in: Analysis of Neurophysiological Brain Functioning, ed C. Uhl, Springer Series in Synergetics (Springer-Verlag, Berlin), pp. 252–273.

[59] Niedermeyer, E., and da Silva, F. L. (1972) Electroencephalography – Basic Principles, Clinical Applications and Related Fields (Urban & Schwarzenberg, Baltimore, 2nd edition).

[60] Cohen, D. (1972) Science **175** 664–666.

[61] Ahonen, A., Hämäläinen, M., Kajola, M., Knuutila, J., Lounasmaa, O., Simola, J., Tesche, C., and Vilkman, V. (1991) IEEE Trans. Magn. **27**, 2786–2792.

[62] Hämäläinen, M., Hari, R., Ilmoniemi, R., Knuutila, J., and Lounasmaa, O. (1993) Rev. Mod. Phys. **65**, 413–497.

[63] Volkmann, J., Joliot, M., Mogilner, A., Ioannides, A., Lado, F., Fazzini, E., Ribary, U., and Llinás, R. (1996) Neurology **46**, 1359–1370.

[64] Saul, J. (1991) in: Rhythms in Physiological Systems, eds H. Haken and H. Koepchen, Vol. 55 of *Springer Series in Synergetics* (Springer,Berlin Heidelberg), pp. 115–126.

[65] Anrep, G., Pascual, W., and Rössler, R. (1936) Proc. Roy. Soc. (London) Ser. B **119**, 191–217.

[66] Anrep, G., Pascual, W., and Rössler, R. (1936) Proc. Roy. Soc. (London) Ser. B **119**, 218–230.

[67] Schmidt, R., and Thews, G. (1983) Human Physiology (Springer, New York, 1983).

[68] Press, W. H., Teukolsky, S. T., Vetterling, W. T., and Flannery, B. P. (1992) Numerical Recipes in C: the Art of Scientific Computing (Cambridge University Press, Cambridge).

[69] Palus, M. (1997) Phys. Lett. A **227**, 301–308.

[70] Theiler, J., Eubank, S., Longtin, A., Galdrikian, B., and Farmer, J. (1992) Physica D **58**, 77–94.

[71] Kurths, J., and Herzel, H. (1987) Physica D **25**, 165.

[72] Schreiber, T., and Schmitz, A. (1997) Phys. Rev. Lett. **77**, 635–638.

[73] Landa, P., and Zaikin, A. (1996) Phys. Rev. E **54**, 3535–3544.

[74] Schack, B. (1999) in: Analysis of Neurophysiological Brain Functioning, ed C. Uhl, Springer Series in Synergetics (Springer-Verlag, Berlin), pp. 230–251.

[75] Miltner, W., Braun, C., Arnold, M., Witte, H., and Taub, E. (1999) Nature **397**, 434–436.

[76] Kwapien, J., Drozdz, S., Liu, L., and Ioannides, A. (1998) Phys. Rev. E **58**, 6359–6367.

[77] Panter, P. (1965) Modulation, Noise, and Spectral Analysis (McGraw–Hill, New York).

[78] Smith, M., and Mersereau, R. (1992) Introduction to Digital Signal Processing. A Computer Laboratory Textbook (Wiley, New York)

[79] Boashash, B. (1992) Proc. of the IEEE **80**, 520–568.

[80] Feldman, M. (1994) Mechanical Systems and Signal Processing **8**, 119–127.

[81] Little, J., and Shure, L. (1992) Signal Processing Toolbox for Use with MATLAB. User's Guide (Mathworks, Natick, MA).